

16.851: Satellite Engineering

Portfolio

Fall 2003

Bill Nadir

Table of Contents

LEARNING OBJECTIVES	3
REFLECTIONS	3
PROBLEM SET 1: POWER SYSTEM DESIGN AND TRADE STUDY FOR A SATELLITE KILLER SPACECRAFT	4
PROBLEM SET 2: STUDY OF ORBITAL MINEFIELD FROM ROGUE STATE	13
PROBLEM SET 3: DESIGN MODULE FOR A SPACECRAFT ATTITUDE CONTROL SYSTEM	42
PROBLEM SET 4: EFFICIENT ORBIT TRANSFER: USE OF ELECTRIC PROPULSION FOR ORBIT RAISING	65
PROBLEM SET 5: SPACE HOTEL DESIGN: PRELIMINARY STRUCTURAL DESIGN AND COST ESTIMATION	87
PROBLEM SET 6: DESIGN OF AN ARTIFICIAL GRAVITY MARS MISSION	103

Learning Objectives

The main objectives for my learning in Satellite Engineering were to do significant research on many spacecraft subsystems, learn how they work together, improve my technical writing skills, and improve my abilities to work in a group. Other learning objectives included improving my research abilities and learning more about tradeoffs between various spacecraft subsystems. Finally, I desired to share my knowledge and experience from working for the previous two years at Boeing Satellite Systems in El Segundo, CA with other students in the class to help them understand the “real life” aspects about satellite engineering.

Reflections

In working on the various problem sets throughout the semester, I had the opportunity to perform in-depth research on a variety of topics related to spacecraft engineering. I researched topics such as lasers, space debris, how to support human life in space, attitude control systems, spacecraft shielding from radiation and debris, and cost modeling. Before enrolling in 16.851, I had limited knowledge on these topics, but I now have a more in-depth understanding of them.

Working in a different group for each problem set was a challenge, but it definitely paid-off in the end. I had the experience of working with new people every two weeks on a project. This forced me and other students to meet new people and learn how to schedule meetings, tasks, and delegate work under somewhat stressful circumstances. Friends were made as a result of this process as well as other contacts which may be beneficial in the future.

I had intended to put many of my engineering skills learned while working at Boeing to use in Satellite Engineering, but that turned out not to be the case. Other than using my CAD skills, many of my skills at structures and antenna design were not of any use in the problem sets for this class.

Overall, I learned a great deal about spacecraft systems engineering from 16.851 as well as gained valuable experience from the class. This portfolio contains the problem sets I was involved in working on as well as a summation of the software modules created. Finally, this portfolio details useful references found during the researching phase of each problem set.

Problem Set 1: Power System Design and Trade Study for a Satellite Killer Spacecraft

Summary

The purpose of this problem set was to investigate the power system design trades involved in the engineering of a satellite designed to disable enemy satellites in Low Earth Orbit (LEO) using a laser. Based on the power requirements of the laser and the constant power requirements for the remainder of the spacecraft, the solar arrays and batteries for the spacecraft were sized.

Various laser firing scenarios and battery/solar array designs were investigated to see which power system design is the most mass efficient. The number of laser firings per orbit was varied. Also, the possibility of only sending power to the laser from the batteries versus generating enough power constantly from the solar cells such that no battery power was required was investigated.

Results

After the analysis was complete, it was found that the optimal power system configuration was to draw 100% of the laser firing power from the batteries. In addition, it was determined that the lowest power system mass per laser firing was to fire the laser four times per orbit rather than one or two firings.

Useful References

This problem set involving only one spacecraft subsystem relied almost completely on *Space Mission Analysis and Design* by Wertz and Larson. Chapters 10 and 11 were used extensively for battery sizing, solar cell sizing, and other power system design procedures.

Power System Design and Trade Study for a Satellite Killer Spacecraft

Names withheld

Massachusetts Institute of Technology, Cambridge, Massachusetts 02139

A military “Satellite Killer” spacecraft is to be put into a Low Earth Orbit at an altitude of 600 km. It will have an average power requirement of 600 W during daylight and eclipse. In action it should be able to fire a 10 kW laser at a target enemy satellite in a similar a LEO. It is to be operational for five years.

First determine how the laser could be used to disable the target satellite. Next, investigate various power system designs that meet the requirements, taking into account the degradation of the system over mission duration. Compare different power system designs and options and choose one that realizes the best compromise between the following factors: mass, and frequency of firings. Ignore orbit adjustment requirements to maneuver the “killer” spacecraft within striking range of its target. Also, ignore any laser refueling requirements and any laser tracking/pointing requirements.

Nomenclature

A_{CL}	= Solar array area required for charging batteries with power to fire laser	t_c	= Battery charging time
A_{PL}	= Solar array area required for powering laser directly	t_{cl}	= Laser battery charging time
A_{sa}	= Solar array area required to power satellite (not including laser) for one full orbit	T_e	= Eclipse time
A_{tar}	= Area of the target spotted by the laser	T_d	= Time the S/C is in the sun (“day” time)
C_r	= Required battery capacity	t_f	= Laser firing time
C_{tar}	= Average calorific capacity of the target	X_{cl}	= Efficiency of electrical path from solar arrays to batteries
DOD	= Battery depth-of-discharge	X_e	= Efficiency of electrical path from solar arrays to batteries and to laser
E_{cl}	= Energy required from solar cells to charge up laser batteries between two firings	X_d	= Efficiency of electrical path from solar arrays to laser
E_{laser}	= Energy required to fire laser	ΔT_{tar}	= Temperature by which the target is heated up
e_{tar}	= Thickness of the target spotted by the laser	θ	= Angle of incidence of the sunbeams on the solar cells
f_E	= Eclipse fraction	β	= Angle between the sun and orbit plane (Beta angle)
h	= Altitude of Satellite Killer spacecraft	μ	= Gravitational constant * Earth’s mass (constant = $3.986 \times 10^5 \text{ km}^3/\text{s}^2$)
I_d	= Inherent degradation of solar array		
L_D	= Lifetime degradation of solar array		
m_a	= Solar array mass		
m_{batt}	= Mass of batteries		
n	= Transmission efficiency between batteries and laser (assumed to be 0.9)		
N	= Number of batteries		
P	= Orbital period		
P_{CL}	= Power output by solar arrays to charge batteries used by laser		
P_d	= Average power required during “day”		
P_e	= Average power required during eclipse		
P_{laser}	= Power of the laser		
P_0	= Solar array power output		
P_{sa}	= Required solar array power for average S/C power for one orbit		
R	= Radius of Earth		

Introduction

This paper answers the above question by designing the “best” power system for the Satellite Killer spacecraft. Our major assumptions are given in the question. Other assumptions are mentioned in the document as they are needed.

This solution is primarily concerned with designing the power system for the Satellite Killer spacecraft. The design of the laser and supporting hardware is not the focus of this paper. However, an attempt was made to make the laser data used in the design of the power system as realistic as possible.

Our solution to the proposed question is that a power system comprised of solar arrays and batteries is the best choice for the Satellite Killer. In addition, the most efficient use of mass for this power system is determined. This directly influences the laser firing rate per orbit. A firing rate of 4 per orbit was found to be the most efficient use of the Satellite Killer, based on our assumptions.

Use of the Laser: General Considerations

Lasers are now commonly used in industry to cut metals or other materials. To do so, the beam is focused to create a tiny spot of a power density greater than 100 kW/cm². Such a power density requires a focus on the target that cannot be achieved if the target is not close enough to the laser source. This is not the case for the “Satellite Killer”: it will be shooting at its target from a much greater distance.

The laser would not be used to damage the target in the way an industrial laser does. Instead, it will be used to heat up a larger portion of the target with a smaller power density than the industrial application, but over a much longer period of time. This is to be described later in a more quantitative way.

The equation of heat transfer from the laser beam to the target is the following:

$$P_{laser} t_f = C_{tar} \Delta T_{tar} A_{tar} e_{tar} \quad (1)$$

It has been assumed here that all the power from the laser source is transferred to the target. The loss of energy of the target by radiation has also been ignored, which will be justified by the value of A_{tar} . C_{tar} will be given equal to 1.6 MJ.K⁻¹.m⁻³, which is the average value for metals. In the next paragraph, we will explain the choices that we have made for the values of ΔT_{tar} , A_{tar} and e_{tar} .

Quantitative Design of the Laser

The aim of the firing is to heat up the target (or some part of it) by a sufficient temperature in order to disable it. Hence, the spacecraft should shoot at the target as it is in daylight, when its temperature is at a maximum. We will choose to heat it up by $\Delta T_{tar} = 200^\circ\text{C}$. Typical solar cells have an upper limit operating temperature of around 100-120°C. The temperature of the cells after the laser hits the target will be nearly 200°C hotter than this upper temperature limit. This should be enough to severely damage some fragile parts of the solar array.

In order to hit a part of the target as wide as possible, the diameter of the beam will be chosen equal to the average width of the target, which is about 1.5 meters. This corresponds to $A_{tar} = 1.77 \text{ m}^2$. This target size was determined by assuming the size of the target satellite’s solar array. The width of the rectangular-shaped array may be approximately 1.5 m and several firings of the laser may be required to fully disable the target satellite’s power source.

Note that we will need an appropriate optical system adapted to the laser to create a 1.5 meter spot on the target; calculations of diffraction would show that we would need a 60 cm lens to do so from 400 km away. This lens diameter dramatically increases with the distance to the target, which is the reason why the Satellite Killer and target satellite need to be in similar orbits. This allows the Satellite Killer to shoot at a relatively close range (less than 400 km).

The value of A_{tar} also implies a power density of 5,650 W/m²; this is much higher than the power density of natural radiation from the spacecraft. This value is given by Stephan-Boltzmann’s equation, and would be around 100 W/m². Therefore, it is a correct assumption to ignore radiation cooling of the target in equation 1.

As for the value of e_{tar} , it has been chosen equal to 1 cm. Since the beam would most likely be aimed at a region of the target with a large surface area, perhaps at its solar arrays, one might think that e_{tar} should be taken equal to the thickness of the solar cells. As a matter of fact, the duration of shooting that is calculated later is not short enough to ignore cooling of the target solar array surface by conduction through the arrays structure. To take this into account, we shall consider the actual thickness of the solar arrays being heated up to be $e_{tar} = 1 \text{ cm}$.

Firing Energy Requirements

Now that the values of the different parameters in equation 1 have been chosen, we can re-formulate this equation to calculate the firing duration:

$$t_f = \frac{C_{tar} \Delta T_{tar} A_{tar} e_{tar}}{P_{laser}} \quad (2)$$

which turns out to be equal to approximately 1 min. Knowing this figure, we are now able to determine the total amount of energy required to fire the 10 kW laser, E_{laser} :

$$E_{laser} = P_{laser} t_f \quad (3)$$

We can infer from equation 3 that $E_{laser} = 170$ W.hr. This value, along with the value of P_{laser} , is the key to the design of the power system associated with the laser.

Investigation of Solar Array and Battery Power Source

The first power system design to be studied is comprised of solar arrays and batteries. For this power system design, the Sun is the primary power source. Several sections to follow document the calculations used to size the appropriate solar power system for the Satellite Killer spacecraft.

Calculation of Eclipse Time

The first equation used in the calculation of the eclipse time of the Satellite Killer spacecraft is the eclipse fraction, shown in equation 4.

$$f_E = \frac{1}{\pi} \cos^{-1} \left[\frac{\sqrt{h^2 + 2Rh}}{(R+h)\cos\beta} \right] \quad (4)$$

Since the maximum eclipse fraction is required for this study, the beta angle, β , is assumed to be equal to zero. The resultant equation can be seen in equation 5. The solution for the orbit of the Satellite Killer is shown in equation 6.

$$(f_E)_{\max} = \frac{1}{\pi} \cos^{-1} \left[\frac{\sqrt{h^2 + 2Rh}}{(R+h)} \right] \quad (5)$$

$$(f_E)_{\max} = \frac{1}{\pi} \cos^{-1} [0.406] = .367 \quad (6)$$

Once the eclipse fraction has been determined, the orbital period, P , must be calculated. This is shown in equations 7 and 8.

$$\text{mean motion} = \sqrt{\frac{\mu}{a^3}} = \sqrt{\frac{\mu}{r^3}} = .00108 \frac{1}{s} \quad (7)$$

$$P = \frac{2\pi}{\text{mean motion}} = 96.68 \text{ min} \quad (8)$$

Now that the orbital period and eclipse fractions have been found, the maximum eclipse period, $T_{e_{\max}}$, can be calculated using the following equation.

$$T_{e_{\max}} = P(f_E)_{\max} = 35.48 \text{ min} \quad (9)$$

Selection of Solar Cell and Battery Types

The two major types of available solar cells are made of silicon (Si) and gallium arsenide (GaAs). For the purposes of this study, the GaAs solar cells have been chosen. The performance and degradation rate of the GaAs cells is significantly better than the Si cells. Table 1 below illustrates this.

Table 1 Comparison of Si and GaAs Solar Cells

Cell Type	Performance (W/m ²)	Degradation per Year (%)
Si	190	3.75
GaAs	244	2.75

The decision about which battery to use was primarily made by comparing the specific energy densities of space-qualified secondary batteries. Based on the data shown in Table 2, nickel hydrogen (NiH₂) batteries were chosen to be used for this spacecraft.

Table 2 Battery comparison

Battery Type	Specific Energy Density (W*hr/kg)
Nickel cadmium	25-30
Nickel hydrogen (individual pressure vessel design)	25-40
Nickel hydrogen (single pressure vessel design)	43-57

Solar Array Sizing for S/C Average Power Requirements

The solar arrays necessary to provide power for the entire spacecraft except the firing of the laser are sized in this section. The additional solar arrays needed to power the laser are sized in a later section. The solar arrays for the "Satellite Killer" are assumed to be of the deployed planar array type.

A beginning-of-life (BOL) efficiency of the GaAs solar arrays is assumed to be 0.18.¹ The solar illumination intensity on the planar solar arrays is assumed to be 1358 W/m². Also, the inherent degradation of the solar cell power transfer is assumed to be a factor of 0.77. Therefore, the estimated BOL power output of the GaAs solar cells, P₀, can be calculated. This is shown in equation 10.

$$p_0 = (0.18)(1358 \frac{W}{m^2})(0.77) = 187.9 \frac{W}{m^2} \quad (10)$$

We then need to reduce the value of P₀ because the angle of the radiation of the sun onto the solar panels is not perfectly normal. The following equation is used to make this correction.

$$(p_0)_{BOL} = p_0 I_d \cos(\theta) \quad (11)$$

where p₀ = 244 W/m² for GaAs solar cells, I_d = 0.77, and θ = 20° (worst case), which gives us (p₀)_{BOL} = 177 W/m².

Now that the estimated BOL power output of the solar cells has been determined, the required power the solar array must provide during daylight to power the spacecraft for an entire orbit can be found, P_{sa}.

$$P_{sa} = \frac{\left(\frac{P_e T_e}{X_e} + \frac{P_d T_d}{X_d} \right)}{T_d} \quad (12)$$

A direct energy transfer power control system has been chosen for the purposes of this study, so the values of X_e and X_d are .065 and .085, respectively.¹ Once the values for the required spacecraft power, time of day, and time of eclipse are put into equation 11, the required solar array power is determined. This is shown in equation 13.

$$P_{sa} = 1241W \quad (13)$$

The solar cell lifetime degradation is required to determine the solar array area needed to provide the required power at EOL. This estimated degradation term is calculated using equation 14.

$$L_d = (1 - \text{deg radiation} / \text{yr})^{\text{satellite life}} = .87 \quad (14)$$

Using the degradation term above, the EOL power output of the solar cells can be determined. This is shown in equation 15.

$$(p_0)_{EOL} = (p_0)_{BOL} L_d = 154 \frac{W}{m^2} \quad (15)$$

Next, the EOL solar array area required for spacecraft average power can be determined. This is shown below.

$$(A_{sa})_{EOL} = \frac{P_{sa}}{(p_0)_{EOL}} = 8.1m^2 \quad (16)$$

Therefore, 8.1 m² of solar cells are required to provide 600 W of power to the spacecraft during daytime and eclipse.

The mass of the planar solar arrays is estimated using equation 16.³ The resultant mass of the solar arrays for the spacecraft average power requirements is 49.6 kg.

$$(M_a)_{avg} = 0.04P_{sa} = 49.6kg \quad (17)$$

Battery Sizing for S/C Average Power Requirements

A major assumption made for the battery sizing was the EOL depth-of-discharge (DOD) of the batteries. This value was assumed to be 38%. Also, a specific energy density of 50 W.hr/kg for the NiH₂ batteries is assumed for use in the battery sizing calculations (see Table 2).

The solution for the required battery capacity per battery is shown below in equation 17. Note that the number of batteries, N, has been chosen to be 2 for redundancy.

$$C_r = \frac{P_e T_e}{(DOD)Nn} = 518.7W \cdot hr / \text{battery} \quad (18)$$

Next, the total mass of batteries required to power the spacecraft during eclipse can be determined. This is shown in the following equation.

$$m_{batt} = \left(\frac{C_r}{50 \frac{W*hr}{kg}} \right) N \quad (19)$$

If the battery mass is solved using the required battery capacity, C_r, the battery mass required to power the spacecraft during eclipse, is calculated to be 20.74kg.

Solar Array Sizing for Laser Firing Power Requirements

The Satellite Killer is located in such an orbit that it will be in sunlight for approximately one hour per orbit. Therefore, it is possible to charge the batteries to fire the laser once per orbit or perhaps several times per orbit. The faster the batteries can charge to the energy level required for the laser, E_{laser} , the higher the possible firing frequency of the laser. For the purposes of this study, the charging times of 15, 30, and 60 minutes were investigated. This would allow firing rates of 4, 2, and 1 per orbit, respectively.

Two additional scenarios were studied to find the optimal combination of solar and battery power required to power the laser during firing. One scenario has 50% of the laser power source from batteries (5 kW) and 50% (5 kW) directly from the solar arrays. The third scenario has no power from batteries and 100% (10 kW) of the laser power source from the solar arrays.

In the 100% battery scenario, the following equation gives the relation between the energy required by the laser and the actual energy the solar arrays will have to deliver:

$$E_{cl} = \frac{E_{laser}}{X_{cl}} \quad (20)$$

where $X_{cl} = 0.9$. Hence, by expressing energy as the product of power by duration, we get the actual power requirement on the solar cells:

$$P_{cl} = \frac{P_{laser} t_f}{X_{cl} t_{cl}} \quad (21)$$

We can then calculate the BOL power production capability per unit area of the array:

$$(p_0)_{BOL} = p_0 I_d \cos(\theta) \quad (22)$$

where $p_0 = 244 \text{ W/m}^2$ for GaAs solar cells, $I_d = 0.77$, and $\theta = 20^\circ$ (worst case), which gives us $(p_0)_{BOL} = 177 \text{ W/m}^2$.

Then we get $(p_0)_{EOL}$ by using equation 15. Based on a five-year mission, $(p_0)_{EOL} = 154 \text{ W/m}^2$.

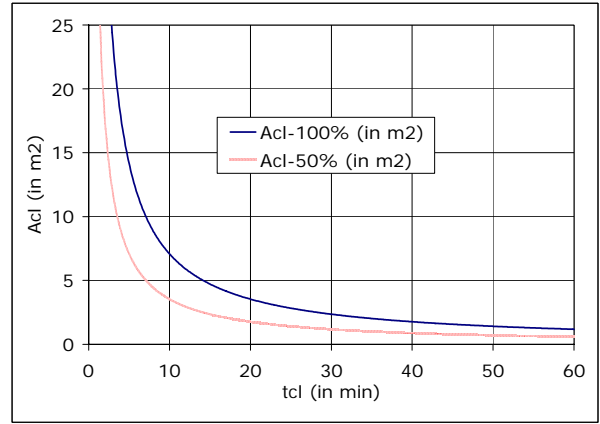
Next, with the help of equation 21, the relation

between the area A_{cl} of solar arrays needed and the charging duration t_{cl} can be determined.

$$A_{cl} = \frac{P_{laser} t_f}{\Omega_{EOL} X_{cl} t_{cl}} \quad (23)$$

A value is then chosen for A_{cl} . This value depends on the number of consecutive times the Satellite Killer can fire its laser during a an approximate 60 min daylight period, as shown in Figure 1 (upper curve).

Figure 1 Relation between charging duration t_{cl} and area of solar cells A_{cl} , in regard of the firing frequency



Note: to get the curve for the 50%-battery scenario (lower curve), P_{laser} has been divided by 2.

Based on the information in Figure 1, the solar array areas required for the different scenarios and various charging times are calculated. The area of the solar arrays required to charge the batteries, A_{CL} , and the area of the solar arrays required to provide direct power to the laser, A_{PL} , are determined. The values for A_{CL} were determined by using the curves in Figure 1. The resulting values are shown in Table 3.

Table 3 shows that the 100% battery charging scenario requires significantly smaller solar arrays than the other two scenarios for all three charging times. This is due to the fact that no solar power is required to directly power the laser. Only battery power is used.

Table 3 Solar array areas for various charging scenarios

% Battery Power / % Solar Power	Battery Charge Time, t_c (min)	$A_{CL}(m^2)$	$A_{PL}(m^2)$	Total Area Required (m^2)
100 / 0	15	6.66	0.00	6.66
100 / 0	30	3.33		3.33
100 / 0	60	1.67		1.67
50 / 50	15	3.33	32.47	35.80
50 / 50	30	1.67		34.14
50 / 50	60	0.83		33.30
0 / 100	15	0	64.95	64.95
0 / 100	30	0		64.95
0 / 100	60	0		64.95

Next, the masses of the solar arrays required for charging the batteries are calculated. First, the power output of these solar arrays must be determined. This is used using equation 24.

$$P_{CL} = \frac{E_{laser}}{t_c} = \frac{P_L t_f}{t_c} \quad (24)$$

Finally, the total masses of the solar arrays required for three proposed scenarios are calculated using equation 17. The results are shown in Table 4. Note that the masses calculated here are only for the portion of the solar arrays used to for laser power.

Table 4 Total mass of solar arrays for powering laser

% Battery Power / % Solar Power	Battery Charge Time, t_c (min)	$(m_a)_{laser}$ (kg)
100 / 0	15.00	29.63
100 / 0	30.00	14.86
100 / 0	60.00	7.41
50 / 50	15.00	214.86
50 / 50	30.00	207.41
50 / 50	60.00	203.70
0 / 100	15.00	400.00
0 / 100	30.00	400.00
0 / 100	60.00	400.00

Table 4 shows that the 100% battery charging scenario requires significantly less mass than the other two scenarios for all three charging times.

Battery Sizing for Laser Firing Power Requirements

In order to size the batteries for the various laser firing power scenarios, the required battery capacity must be determined. Equation 18 is used for these calculations. In addition, the battery mass for each scenario is calculated using equation 19. Once again, two batteries have been chosen for this portion of the energy storage ($N=2$). The results for these calculations are shown below in Table 5. Note that the masses calculated here are only for the portion of the batteries used to power the laser.

Table 5 Required battery capacities and battery masses for various power storage scenarios

% Battery Power / % Solar Power	Battery Charge Time, t_c (min)	Cr ($W*hr/battery$)	$(m_{batt})_L$ (kg)
100 / 0	15.00	243.71	9.75
100 / 0	30.00		
100 / 0	60.00		
50 / 50	15.00	121.86	4.87
50 / 50	30.00		
50 / 50	60.00		
0 / 100	15.00	0.00	0.00
0 / 100	30.00		
0 / 100	60.00		

As seen in Table 5, a significant savings in battery mass is achieved by using solar arrays for a portion or all of the laser power required to fire.

Solar Power System Design Options

Now that the calculations have been made for the various solar power system design options, the various designs can be compared. Mass is an important quantity to compare for space applications. Table 6 below compares the total masses of the solar power system design options considered in this study.

Table 6 Mass comparison of solar power system designs

% Battery Power / % Solar Power	Battery Charge Time, t_c (min)	Total Solar Array Mass (kg)	Total Battery Mass (kg)	Array and Battery Mass (kg)
100 / 0	15.00	79.23	30.49	109.72
100 / 0	30.00	64.46		94.95
100 / 0	60.00	57.01		87.50
50 / 50	15.00	264.46	25.61	290.07
50 / 50	30.00	257.01		282.62
50 / 50	60.00	253.30		278.91
0 / 100	15.00	449.60	20.74	470.34
0 / 100	30.00	449.60		470.34
0 / 100	60.00	449.60		470.34

From Table 6, it is shown that the solar power system designs which use only battery power to power the laser for firing require significantly less mass than the other options.

In addition, the 50%/50% and 0%/100% options are impractical because they require extremely large solar arrays to generate the constant power needed for the laser. Table 3 shows those scenarios requiring over 30 and 60 m² of solar array area, respectively. For a relatively “small” spacecraft like the Satellite Killer, those large array sizes would be difficult to incorporate into the spacecraft design.

Other Power System Design Options

The other major types of power systems to choose from are: nuclear reactors, radioisotope thermoelectric generators (RTGs), and solar thermal dynamic power systems.

Nuclear reactors typically provide large amounts of power (>25 kW) which is more than is required for the Satellite Killer. The excess energy produced by the reactor would need to be dissipated by using large thermal radiators. This is unnecessary. In addition, nuclear reactors would be an unpopular idea for many people on Earth. People would be afraid of having a nuclear reactor flying overhead in LEO. They would be worried what about the possible consequences if the spacecraft reentered the atmosphere with radioactive material onboard. This problem may be avoided, however, if the satellite were a classified military satellites shrouded in

secrecy. Therefore, nuclear reactors should not be used for the power source on the “Satellite Killer” spacecraft.

Radioisotope thermoelectric generators (RTGs), a second alternative to the solar power source for the Satellite Killer spacecraft, are not good power sources for some of the same reasons as the nuclear reactor. People would be worried about having radioactive material orbiting in LEO. In addition, RTGs are much more expensive than both nuclear reactors and solar power systems by nearly a factor of 6.⁴

A solar thermal dynamic power system is another option to power the Satellite Killer. However, this type of power system is more suited to interplanetary missions. Since our satellite will “see” the same amount of sun after every orbit, a simple solar array and battery system should be necessary. A dynamic power system is much more complex system involving heat exchangers and possibly even a nuclear reactor. Therefore, a solar thermal dynamic power system is not recommended to power the Satellite Killer spacecraft.

Conclusion

Based on the sizing done for a solar array and battery power system for the Satellite Killer spacecraft and the lack of other reasonable power system options, the “best” power system to be used is a solar array and battery system.

As seen in Table 6, the “best” solar power system design would be one in which all of the laser power required to fire would come from charged-up batteries (100%/0% scenario). The mass savings makes this design attractive. However, an additional power system design choice needs to be made. The number of laser firings per orbit will vary with the required battery charging time. The charging times of 15, 30, and 60 minutes were investigated. Based on these charging times and since the spacecraft will be in sunlight for approximately one hour per orbit, the satellite has the option of firing the laser one, two, or four times per orbit. The “best” design will be chosen by calculating the power system mass divided by the number of possible firings. The results are shown in Table 7.

Table 7 Mass per laser firing results

% Battery Power / % Solar Power	Battery Charge Time, t_c (min)	Firings per Orbit	Array and Battery Mass (kg)	Mass per Firing (kg)
100 / 0	15	4	109.72	27.43
100 / 0	30	2	94.95	47.48
100 / 0	60	1	87.5	87.50

Table 7 shows that power system mass is used most efficiently if the battery charging time is 15 minutes, resulting in four possible laser firings per orbit. This is the most efficient design by nearly factors of 2 and 4 over the second and third options in the table, respectively.

References

¹Larson, W. and Wertz, J., *Space Mission Analysis and Design*, 2nd Ed., p. 396, paragraph 5

²Larson, W. and Wertz, J., *Space Mission Analysis and Design*, 2nd Ed., p. 404, fig. 11

³Larson, W. and Wertz, J., *Space Mission Analysis and Design*, 2nd Ed., p. 317, eq. 10-11

⁴Larson, W. and Wertz, J., *Space Mission Analysis and Design*, 2nd Ed., p. 393, Table 11-32

Problem Set 2: Study of Orbital Minefield from Rogue State

Summary

The increasing dependence of the United States on space assets expressed the need to investigate the feasibility of a rogue nation of damaging or disabling US space assets in Low Earth Orbit (LEO).

This problem set first involved researching what satellites are in LEO and where they were located. A likely launch vehicle to be used for such an attack was chosen, mines were selected, a mine dispersal device was designed, and software was developed to predict the orbit of the minefield and how it changes over time. Finally, several attack scenarios were investigated to determine the effectiveness of the minefield against current LEO targets.

Results

Once the launch vehicle was selected, the type of mine to use was determined. This selection process was driven by mine size and mine mass. It was desired to have a mine large enough to penetrate existing spacecraft shielding but at the same time be fairly lightweight. In addition, we desired that the mines be commercially available and therefore easy for terrorists to obtain. We settled on BBs as the mines of choice for this exercise.

The mine dispersal device (MDD) was basically a simple structure containing millions of BBs packed around explosives. The amount of explosives required was determined by specifying the initial velocities of the particles after the detonation.

Next, MATLAB code was written to determine how the orbit of the mines changes over time depending on the location of detonation of the minefield. Atmospheric drag was considered in these calculations.

Three attack scenarios were investigated for this project. First, an attack on Iridium satellites was investigated. It was found that we had a 10% chance of hitting a critical zone on an Iridium satellite within the first 30 days after detonation and 85% after 2 years in orbit.

The attack on all LEO satellites was the next attack scenario. This was accomplished by detonating the MDD over the equator. The precession of the longitude of the ascending node allowed the minefield to spread out enough to surround the Earth. Probabilities of 3.1% and 4.3% over one and two years, respectively, were determined to be the likelihood of a mine impacting a satellite in LEO.

The final attack scenario was an attack on the International Space Station. It was found that our “shotgun blast” of mines would likely hit the space station within the first day of detonation, but the probability of hitting a critical system was only about 10%. However, this would likely be too great of a threat to maintain humans on the space station if this scenario was likely to happen.

Useful References

Launch Vehicles

Isakowitz, Steven J., *International Reference Guide to Space Launch Systems*, 3rd Ed., AIAA, 1999.

This reference is the complete guide to all launch vehicles. It contains specifications of each launch vehicle and as much detail as you will find anywhere.

Orbital Debris

Milne, Antony, *Sky Static*, Praeger, 2002,

Johnson, Nicholas L., *Artificial Space Debris*, Krieger Publishing Co., 1991,

Graves, R., *Space Station Meteoroid and Orbital Debris Survivability*, AIAA-2002-1607

These references are useful for researching orbital debris, and the current and future methods being employed to protecting manned and unmanned spacecraft from orbital debris.

Orbital Mechanics

Bate, R., Mueller, D., and White, J., *Fundamentals of Astrodynamics*, Dover Publications, Inc., New York.

Battin, Richard. *An Introduction to the Mathematics and Methods of Astrodynamics*, Revised Edition., AIAA, Reston, VA. 1999.

Chobotov, Vladimir A. (editor), *Orbital Mechanics*, Third Edition, AIAA Educational Series, Reston, VA, 2002.

Study of Orbital Minefield from Rogue State Feasibility Analysis and Defense Mechanisms

16.851 Satellite Engineering

*Massachusetts Institute of Technology, Cambridge, MA
October 2003*

Motivation

Since 2001, the Pentagon has warned that reliance on space technology is America's Achilles heel. Countries such as China and Russia are known to have programs underway to develop "means to disrupt, degrade, or defeat portions of the U.S. space support system."¹

To this day, orbital debris has been mostly a nuisance to U.S. space assets. However, it may be possible for an enemy of the United States to develop a method of significantly damaging space assets by intentionally injecting a debris field into orbit. Understanding how such a debris field could be created and how it would affect space assets is a necessary and vital task.

Problem Statement

Study the threat of a rogue state "mining" low-Earth orbit (LEO) by utilizing one Delta IV Medium+ equivalent launch vehicle (near equivalent to China's Long March CZ3B).

Introduction

Orbital debris has been a growing nuisance for the space community ever since man began launching objects into space in the mid-20th century. Increasingly, orbital debris is taken into consideration when a satellite is designed. Mission planners specify requirements for the satellite to be able to survive a certain size and frequency of debris impacts. The design impact of orbital debris has been minimized due to engineering efforts.

The purpose of this study is to determine if it is feasible for a foreign nation to deliberately create an orbital debris field in LEO with the intention of severely damaging US space assets. This may be a method for a foreign nation to try to gain ground on the lead the United States currently has in the area of space assets and technology.

Significant investigation is made to determine an approach that would effectively "mine" LEO. The mines chosen for the purposes of this study are off-the-shelf, inexpensive BBs. The mines are dispersed in orbit by launching a Mine Dispersal Device (MDD), which deploys the mines at the required orbital location. The mines are launched into a retrograde orbit so their relative velocity with respect to their target is roughly twice the circular speed at the target altitude. In LEO, that means a relative velocity of approximately 15 km/s.

There are hundreds of vulnerable satellites in LEO that are within striking distance of the MDD. The International Space Station, the Hubble Space Telescope, and the Space Shuttle are several high-profile targets to be found in LEO. Several communications constellations orbit in LEO as well. Iridium and OrbcComm inhabit the higher regions of LEO around 800km in altitude. There are also many weather and research satellites orbiting in LEO. Figures 1 and 2 are a survey of the altitudes and inclinations of satellites in LEO, based on current orbital elements from the Satellite Toolkit (STK).

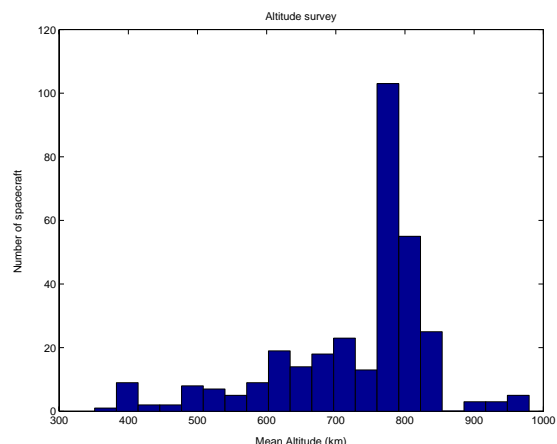


Figure 1 LEO S/C altitude survey

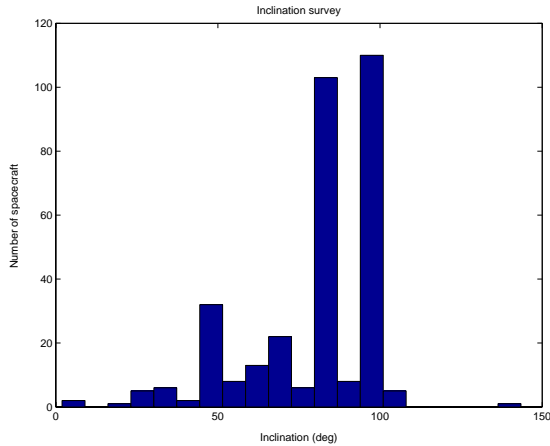


Figure 2 LEO S/C inclination survey

Figure 1 shows that most LEO satellites are orbiting between 750 and 850 km altitude. Figure 2 shows that most of these same satellites have inclinations around 90 (polar) to 97 (sun-synchronous) degrees. There are also a significant number of satellites orbiting at around 50 degrees inclination.

Three “attack scenarios” are investigated in this study. First, an attack on a group of polar-orbiting spacecraft is investigated. Next, an attack on nearly all LEO spacecraft is formulated. Finally, a method of attacking the International Space Station (ISS) is studied.

Methods to defeat or neutralize the enemy minefield are examined. Effectiveness of current spacecraft shielding and possible use of current technology to provide additional protection when required are investigated for their effectiveness against the minefield.

Launch Vehicle Selection

A Delta IV Medium+ (5, 4) launch vehicle was selected for the purposes of this study. This vehicle was selected based on its similarity of launch capability to the Chinese-built Long March CZ3B launch vehicle. It was assumed that launch vehicle data would be easier to obtain for a US-built launch vehicle as opposed to a Chinese-built launch vehicle. Both launch vehicles have the same payload capability of 13,600 kg for a 185 km altitude, 28.5 degree inclination, circular orbit. Therefore, the Delta IV Medium+ (5, 4) launch vehicle is used throughout the rest of this paper in place of the Long March CZ3B.

Table 1 shows the Delta IV Medium+ (5, 4) launch vehicle payload mass capabilities for the three attack scenarios covered in this study.

Table 1 Delta IVM+ payload capabilities²

Attack Scenario	Altitude (km)	Inclination (deg)	Payload Capability (kg)
ISS	380	51.6	5000
Iridium/Other	780	90.0	10000

Please note that the launch to attack the ISS is a retrograde launch. This means the launch vehicle will be placed into an inclination of 128.4 degrees. Since no data has been provided by the launch vehicle manufacturer about the retrograde launch capability of their launch vehicle, and launch vehicle calculations are outside the scope of this paper, it will be assumed that the launch capability to a retrograde orbit to attack the ISS will be roughly half that of the capability to a polar orbit (10,000kg). This results in a retrograde capability of 5,000 kg as seen in Table 1.

Table 2 shows the payload volume capabilities for the two types of fairings used on Delta IVM+ launch vehicles.

Table 2 Delta IVM+ fairing volume options³

Fairing Type	Available Payload Volume (m ³)
4-meter dia.	75.0
5-meter dia.	270.6

Based on the information provided for the Delta IV Medium+ (5,4) launch vehicle, the capability of the vehicle to deliver mines could now be determined.

Mine Selection

A major factor in the selection of mines to be used in this study was the availability of mine materials. In other words, the mines could be easily procured by a rogue state. Therefore, it was decided to use simple, off-the-shelf objects to launch into orbit to act as mines. The objects used for this study are spherical, 6mm diameter, 0.2 gram, metallic BBs.

Mine Effectiveness

The size of the BBs was determined by two constraints. First, the mines must be undetectable from ground tracking stations. It is known that “pieces of space debris that are larger than 10cm ... present no problem because they can be observed from the ground and the crew can take avoiding action.”⁴ Since the BBs used as mines for this study are less than 10 cm in diameter, the

minefield created would be undetectable from any current ground tracking station. Next, the mines must impact the target with enough energy to damage or destroy it. The benchmark used in this study to determine if the mine can damage or destroy the target is if it can penetrate solid aluminum to a depth of approximately 1cm. This number was chosen because most spacecraft structures are made of aluminum and will have an outer wall of a thickness much less than one centimeter, so the mine will penetrate the satellite and cause internal damage. In order to determine the approximate penetration depth of the mines, the Summer equation is used.⁵ This equation is shown below.

$$\frac{P}{d} = 2.28 \left(\frac{\rho_P}{\rho_T} \right)^{2/3} \left(\frac{V}{c} \right)^{2/3} \quad (1)$$

In Equation 1, P is the penetration depth, d is the diameter of the orbital debris object, ρ_P is the density of the orbital debris object, ρ_T is the density of the target material, V is the relative velocity of the debris, and c is the speed of sound in the target material (5.1×10^6 for aluminum). Solving for the penetration depth, it is found that the BBs selected for the minefield in this paper can penetrate solid aluminum to a depth of 1.6 cm. This exceeds the benchmark of 1 cm and therefore these mines are capable of damaging or destroying the target. However, the Summer equation used here may be very conservative. "NASA found that a piece of aluminum debris less than 1 mm had smashed through an aluminum wall 2.5 cm thick."⁶

One important consequence of using spherical-shaped objects as mines is the ability to pack them inside the launch vehicle. When spheres are packed together as densely as possible, some void will remain. The remaining void issue has been addressed in the Kepler Problem. According to Kepler, the densest packing of spheres possible is 74.048% of a given volume.⁷

Mine Dispersal Device (MDD)

The purpose of the MDD is to contain explosives and mines, fit inside the required launch vehicle fairing, survive launch, and detonate the explosives at a specified location in orbit to deploy its payload of mines.

The MDD has three main components. First, it has a structure which contains the payload and mates with the payload adapter of the launch vehicle. Second, the structure of the MDD contains millions of BBs being used as mines. Third, a core of explosives is in the MDD at the core of the mines. Based on the fact that the 4-meter diameter launch vehicle fairing can contain

approximately 491 million BBs and no more than 50 million BBs are used in any of the attack scenarios in this paper, it is clear that the fairing can easily accommodate the required MDD volume.

The fact that only a small portion of the fairing volume is being used for the MDD demonstrates that mass limits the size of the MDD to a much greater extent than fairing volume. Although only a small fraction of the available fairing volume is being used for the MDD, the MDD maximizes the mass launch capability of the launch vehicle selected for this study.

The structure of the MDD will most likely be a lightweight sack or tube which will only be required to keep the mines and explosives together until detonation. The detailed design of the MDD canister is left as future work. Being so lightweight, the mass of the structure of the MDD is assumed to be insignificant compared to the overall total mass of the MDD. This structural mass will be neglected for the remainder of this paper.

The mines are packed around a core of explosives which detonate in orbit to induce the scattering of the mines. This scattering allows the mines to spread out quickly and become a hazard to a large volume of space in LEO. The amount of explosives to be used depends on the number of mines in the MDD. While the actual design of the explosive device is also left as future work, energy equations are used to approximate how much explosive to use for each attack scenario. The chemical energy in TNT is equated to the kinetic energy imparted on the mines. Equation 2 below is the main equation used for this calculation.

$$\frac{1}{2} m_m v_0^2 = m_{TNT} E_{TNT} \quad (2)$$

Here v_0 is the initial velocity, m_m is the mass of the mines, m_{TNT} is the mass of the explosive, and E_{TNT} is the specific energy of the explosive. The initial velocity, v_0 , chosen to impart on each mine is 300 ft/s. This number was chosen because it is a 1-sigma representation of the approximate speed of a bullet fired from a gun, 900 ft/s. This guarantees that 3-sigma, or 99.73% of the mines will have initial velocities less than 900 ft/s. Knowing the energy stored in TNT is 4.689 MJ/kg and the number of mines to be used in each attack scenario, the mass of TNT required can be determined. The results are shown below in Table 3.

Table 3 TNT mass required for attack scenarios

Attack Scenario	Number of Mines ($\times 10^6$)	Mass of Mines (kg)	Required TNT Mass (kg)
1 and 2	50	10000	8.9
3	25	5000	4.5

As can be seen from Table 3, the mass of TNT required is insignificant compared to the total weight of the MDD shown in Table 1. For the purposes of this study, the mass of explosives will be neglected for the remainder of this paper.

Attack Scenario #1: Iridium Satellites

The Iridium satellite constellation is used primarily by the US military and the Department of Defense for global telephone communications. The satellites in this constellation are located in polar orbits and at 780 km altitude.⁸

Iridium satellites were picked as a target because they are well-known and are a good example of a type of satellite a rogue nation may want to destroy in LEO. There are many other satellites in similar orbits such as Landsat, ICESat, and Orbcomm. These satellites are used for research, communications, and other purposes.

Target Size

In order to find the size of the target to strike, a crude estimation of the size of the Iridium satellite bus was made from pictures found of the satellite.⁹ This estimation showed that one side of the triangular-shaped Iridium bus had an area of 2.58 m². However, a strike inside this area will not necessarily hit vital components of the spacecraft that would disable or destroy it. Therefore, the assumption is made that roughly 50% of the total area of the side of the Iridium bus is protecting vital, mission-critical components. Thus, components such as batteries, fuel tanks, computers, and ACS are assumed to fill an area of about 1.29 m².

Attack a Polar Orbit (Iridium)

The MDD is used in this attack scenario to pose a serious threat to polar orbiting satellites in one specific polar orbit. An Iridium satellite is located in such an orbit. The minefield will also pose a smaller threat to other orbiting spacecraft which intersect the orbit of the minefield.

The launch capability of the Delta IV Medium+ (5, 4) launch vehicle is 10000 kg to a 780 km circular, polar orbit.¹⁰ Therefore, it is possible to pack 50 million

mines into the launch vehicle. Please note that all figures generated using MATLAB only display 10,000 mines. This allows the Matlab figures to clearly display the distribution of the minefield in orbit. All numerical results use the actual number of mines.

The MDD is launched into a retrograde orbit in order to maximize the relative velocities of the mines and target. Since this attack involves launching into a polar retrograde orbit, there is no impact on the payload capability of the launch vehicle.

The MDD is detonated over the North or South Pole to result in a “ring” shape of mines focused on the target polar orbit. With the MDD detonation at the pole, the inclination angle of every particle is 90 degrees, regardless of initial conditions. Thus, even though the argument of periapse does change, the longitude of the ascending node is constant (see Equation 24). This prevents the mines from spreading out to completely encapsulate the Earth.

Minefield After 30 Days

Figure 3 shows the distribution of mines in orbit 30 days after being detonated over one of the poles. Please note that the black circle in the figure shows the targeted orbit for this attack scenario.

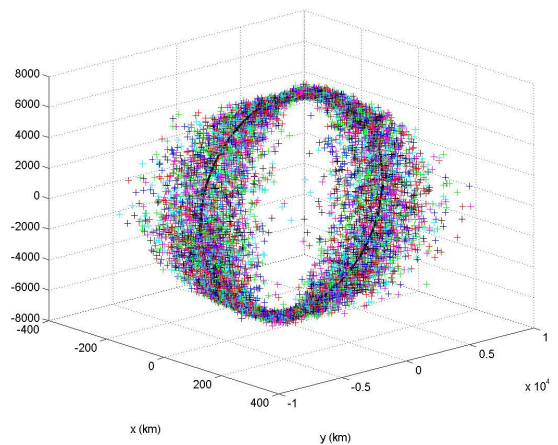


Figure 3 Minefield after 30 days

It can be seen in Figure 3 that the mines have spread out to completely fill the targeted polar orbit. Also note the “necking” effect at the top and bottom of the plot. Those locations are the North and South poles. The mines do not appear to be spreading out much at those locations because the precession of the argument of periapse has no visible effect in polar orbits. The “amount” of spreading out of the mines through various orbit altitudes can be seen in Figure 4, below.

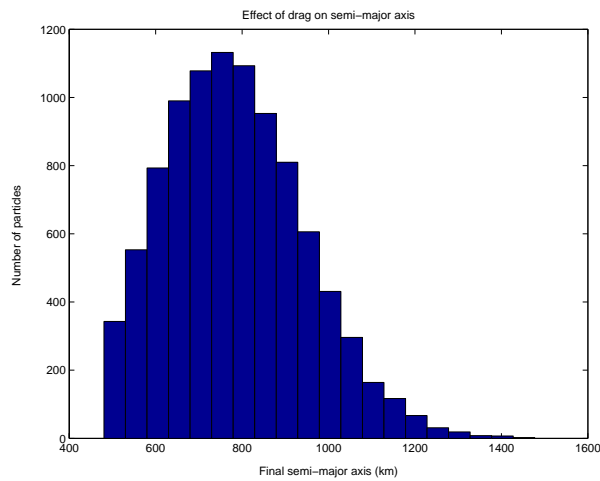


Figure 4 Semi-major axes of mines after 30 days

In addition to the initial dispersal of mines from the MDD detonation, a major contributor to the spreading out of the mines through various altitudes is atmospheric drag (see Equation 26). Even after 30 days, some mines have moved to orbits around 500km in altitude. In fact, 5% of the mines have reentered the Earth's atmosphere at this point.

Despite the initial change in velocity caused by the explosion, the orbits of the mines are still largely circular. This is typical of all of the scenarios presented in this report, and can be seen in Figure 5 for the present case.

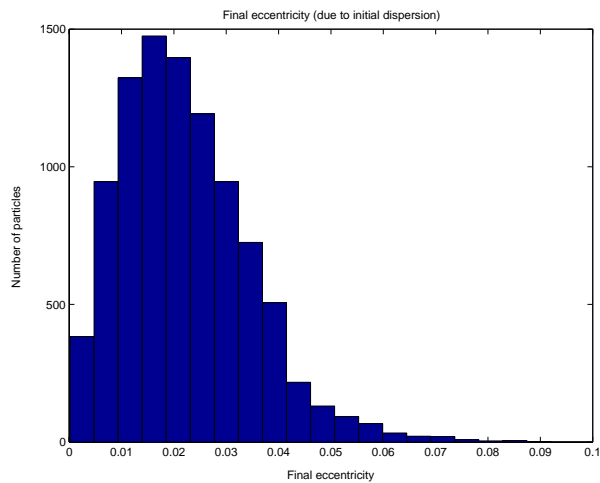


Figure 5 Eccentricities of mines after 30 days

The equation to determine the probability of impacting the target (Equation 29) requires the spatial density of the orbital debris. The spatial density has a major impact on the probability of striking the target. In order to achieve realistic probability numbers, the volume of the disk used to determine the spatial density of the minefield was refined from the total volume to a 3-

sigma volume (refer to software description for details). This 3-sigma volume contains approximately 99.73% of all particles in the minefield. The following three figures show the difference between the total minefield volume and the 3-sigma volume. The outer, red curves denote the total volume limits and the inner, blue curves denote the 3-sigma volume limits.

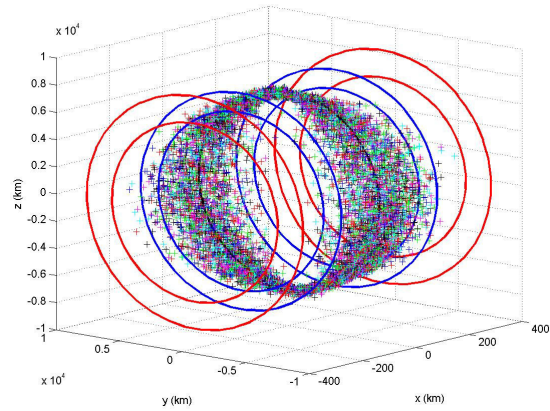


Figure 6 Isometric view of minefield disk volume limits

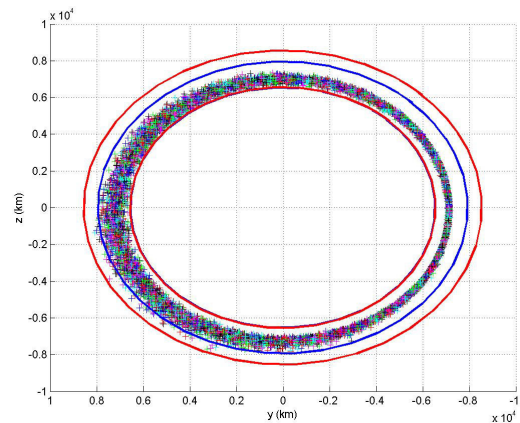


Figure 7 Side view of minefield disk volume limits

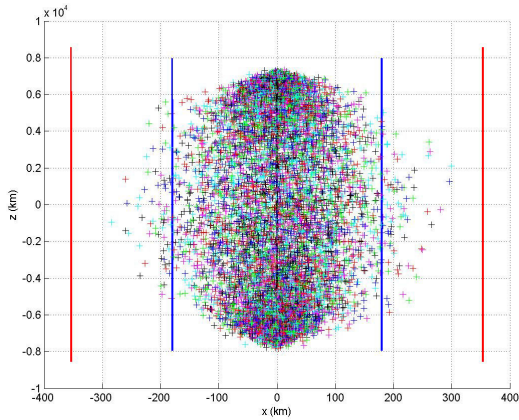


Figure 8 Front view of minefield disk volume limits

It can be seen from Figures 6, 7, and 8 that the difference between the total and 3-sigma volumes is quite significant. Since only a small percentage of mines are present outside the 3-sigma volume, it is much more realistic to use the 3-sigma volume for the probability calculations.

The probability that the targeted Iridium satellite will suffer a critical hit during the first 30 days of the deployment of the minefield is shown in Table 4 below. Please note that the out-of-plane probabilities are for target satellites not in the target orbit but are in other circular orbits which intersect the minefield.

Table 4 Probabilities of impacting target satellite after 30 days

Type of Probability	Probability (%)
In Plane, 3-sigma STD Volume	9.7
In Plane, Total Volume	3.5
Out of Plane, 3-sigma STD Volume	0.2
Out of Plane, Total Volume	0.1

Although the probabilities of impact may seem low, this is the percentage of all satellites in the path of the minefield of being critically impacted by a mine. Even a 9.7% probability could result in the destruction of a number of satellites within a 30-day period. Additionally, this is a statistic for only thirty days, and it will be shown that the minefield will survive for significantly longer than this.

Minefield After 2 Years

The distribution of minefield particles can be seen below in Figure 9. Please note that the black circle in the figure shows the targeted orbit for this attack scenario.

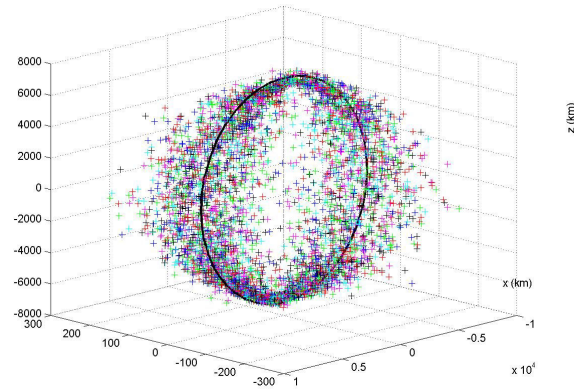


Figure 9 Minefield after 2 years

The minefield after two years looks similar to the picture in Figure 3 of the minefield after 30 days. However, there are significant differences. First, the number of particles shown in Figure 9 is significantly less than that of Figure 3. In fact, 51.5% of the 50 million mines have reentered the Earth’s atmosphere at this point. The second major difference is that the altitudes of the remaining mines have dropped dramatically closer to the Earth’s surface due to drag. The altitudes of the minefield particles after 2 years in orbit can be seen below in Figure 10.

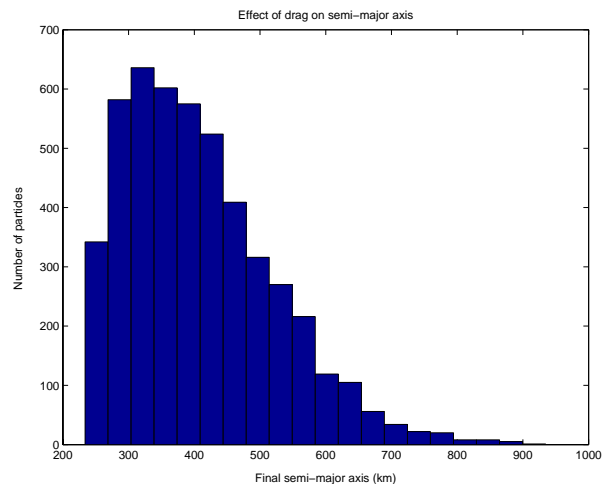


Figure 10 Semi-major axes of mines after 2 years

Figure 10 shows the mines have dropped in altitude significantly during 2 years in orbit. Atmospheric drag has been slowly destroying the minefield over time.

The probability that the targeted Iridium satellite will suffer a critical hit during the first 2 years of the deployment of the minefield is shown in Table 5 below.

Table 5 Probabilities of impact through 2 years

Type of Probability	Probability (%)
In Plane, 3-sigma STD Volume	85.2
In Plane, Total Volume	51.9
Out of Plane, 3-sigma STD Volume	1.3
Out of Plane, Total Volume	1.5

Table 5 shows that the probability of impact over a long time period such as 2 years significantly increases the chances of striking a target spacecraft in the minefield. Theoretically, 85% of all satellites inside the minefield could be disabled or destroyed within two years of the minefield being deployed. Note also that, as the altitude of the minefield is lowered by atmospheric drag, it passes through the less densely populated portions of LEO, potentially damaging that infrastructure as well.

Minefield Effectiveness Over Time

Figure 11 below displays the probability of a critical strike on the targeted Iridium satellite over time. The probabilities in the following figure were calculated using time steps of 30 days. This means that each probability in the plot at a given indicates the probability of strike if a spacecraft were in that minefield for 30 days. This time step was chosen due to the long minefield duration. Please note that the y-axis values are decimal probabilities, not percentages.

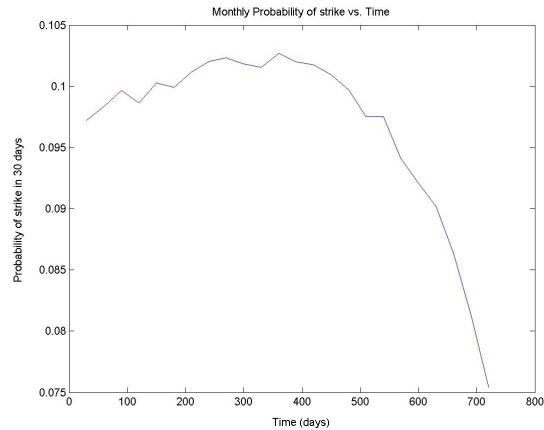


Figure 11 Critical impact probability vs. time

Figure 11 clearly shows that the minefield used to attack the Iridium satellite will present a significant threat until approximately 700 days in orbit. By the end of the 2nd year in orbit, the minefield’s 30-day probability of striking a satellite has decreased dramatically.

It can also be seen in Figure 11 that the probability of a critical strike appears to increase slightly over the 1st year in orbit before the probability begins to decrease. This is caused by the method in which the 3-sigma volume is calculated; after a few months the lowest particles have been removed by the atmosphere while the upper particles have moved very little, causing the calculated volume to decrease and thus the apparent density to increase. There comes a point after around 1 year when the minefield has decayed in altitude too much to remain as much of a threat as it was during the first year in orbit.

Attack Scenario #2: All LEO Satellites

This attack scenario is similar to the previous scenario except the MDD is detonated over the equator. This detonation point allows for the spreading of the minefield throughout the target orbit altitude around the Earth. Since every particle no longer has an inclination of 90 degrees, as seen in Figure 14, the longitude of the ascending node is now free to move. This precession over time results in the Earth being completely surrounded by the minefield.

Minefield After 1 Year

Figure 12 below shows the minefield in orbit after 1 year.

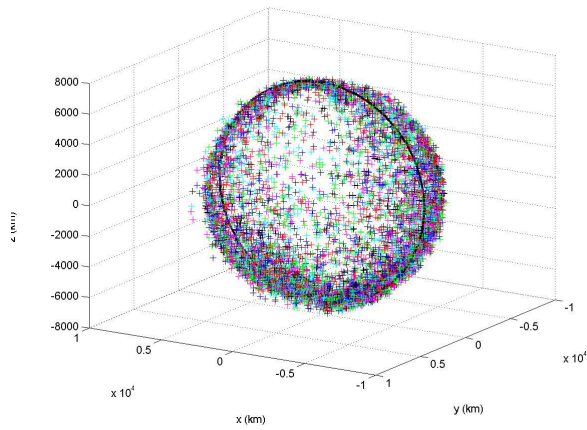


Figure 12 Minefield after 1 year

Figure 12 shows the minefield spread out around the Earth but mostly concentrated in a “ring” shape in the initial polar orbit. Please note that the black circle in the figure shows the targeted orbit for this attack scenario.

Figure 13 shows the effect of drag on the semi-major axes of the mines after 1 year.

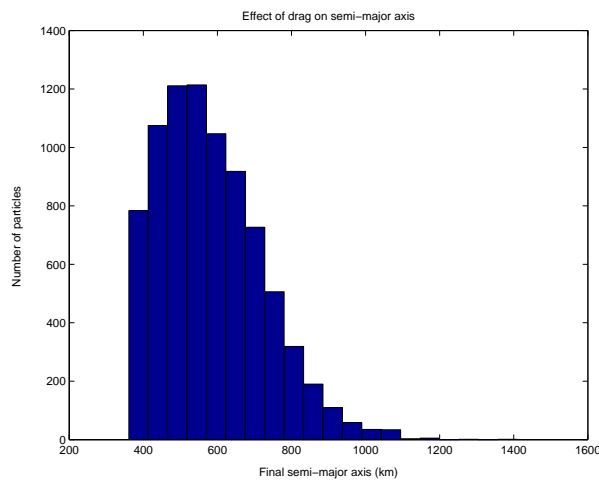


Figure 13 Semi-major axes of mines after 1 year

The altitudes of the mines are shown in Figure 13 to have spread out through most of the altitudes of LEO. Some mines have reentered the Earth’s atmosphere by this point. In fact, 17.6% of the mines have reentered Earth’s atmosphere after 1 year.

Figure 14 shows the distribution of the inclination angle of the individual mines. While the data shown is the result of one year of propagation, the dispersion in inclination is due solely to the initial explosion at the equator.

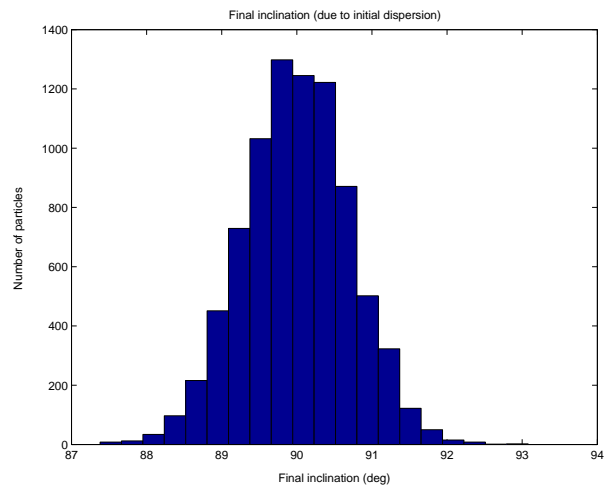


Figure 14 Inclinations of mines after 1 year

The probability that a targeted Iridium satellite will be struck by a minefield particle in a critical area within the first year of this minefield is shown below in Table 6.

Table 6 Probabilities of impact through 1 year

Type of Probability	Probability (%)
In Plane, 3-sigma STD Volume	3.1
In Plane, Total Volume	1.6
Out of Plane, 3-sigma STD Volume	N/A
Out of Plane, Total Volume	N/A

The reason why the out-of-plane probabilities are listed as not applicable in Table 6 is that the purpose of this attack is to spread the mines to form a spherical cloud of mines which surround the Earth. By definition, there are no ‘out-of-plane’ satellites.

The probabilities shown in Table 6 are somewhat low, but it must be mentioned that these percentages are now for nearly all circularly-orbiting LEO satellites. This means that of the hundreds of active LEO satellites, roughly 3% of them could be destroyed within a year of the minefield being deployed. This could have a major impact on the safety of LEO.

Minefield After 2 Years

Figure 15 below shows the minefield particles after 2 years in orbit.

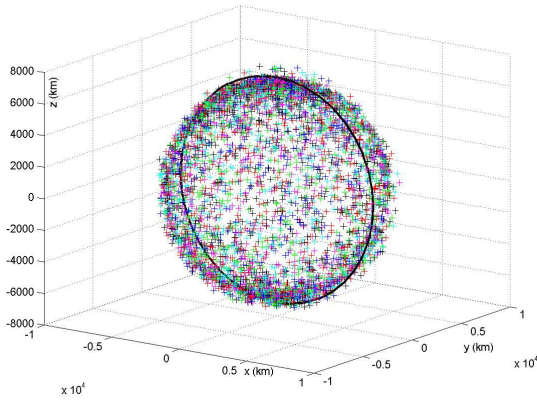


Figure 15 Minefield after 2 years

Figure 15 shows that the minefield is now spread out around the Earth much more than after only 1 year. The minefield can now be seen virtually enclosing the Earth. Please note that the black circle in the figure shows the targeted orbit for this attack scenario.

Figure 16 shows how drag effects the semi-major axes of the mines after 2 years in orbit.

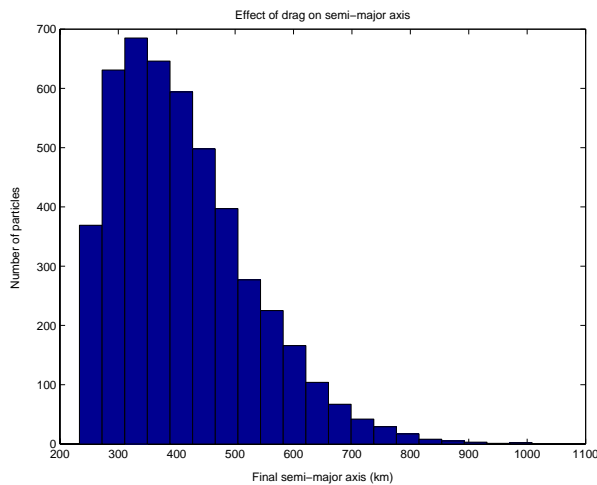


Figure 16 Semi-major axes of mines after 2 years

The altitudes of the mines are shown in Figure 16 to have been lowered due to atmospheric drag effects over 2 years. Many mines have reentered the Earth's atmosphere by this point. In fact, 52.3% of the mines have reentered Earth's atmosphere after 2 years.

The probability that a targeted Iridium satellite will be struck by a minefield particle in a critical area within the first 2 years of this minefield is shown below in Table 7.

Table 7 Probabilities of impact through 2 years

Type of Probability	Probability (%)
In Plane, 3-sigma STD Volume	4.3
In Plane, Total Volume	2.8
Out of Plane, 3-sigma STD Volume	N/A
Out of Plane, Total Volume	N/A

The probabilities shown in Table 7 are somewhat low but still higher than the percentages after 1 year. The probabilities above mean that of the hundreds of active LEO satellites, over 4% of them could be destroyed within 2 years of the minefield being deployed, in this conservative analysis. This could have a major impact on the safety of LEO.

Attack Scenarios 1 & 2: Environmental Impact and Countermeasures

The Iridium satellite target will most likely not survive a direct strike from the minefield on the critical area of the spacecraft bus. Based on the calculations done in the Mine Selection section, it was shown that one of the minefield particles can penetrate 1.6 cm of solid aluminum. An Iridium satellite, or any other communications satellite, will most likely not have thick aluminum shielding to protect the sensitive components of the spacecraft. Adding thick aluminum walls to the spacecraft bus would create a serious mass problem as well as potential thermal and structural problems. Therefore, it is not practical for Iridium or most other satellites in similar LEO orbits to install aluminum shielding to protect their spacecraft from this minefield.

It is also impossible for a ground controller to maneuver the targeted satellite out of the path of the minefield since it is not possible to track 6mm diameter debris particles from the ground.

A Whipple-type shield could be integrated into the spacecraft design, but this type of shield may not protect the satellite either. This type of shield is discussed in detail in the Attack Scenario 3: Environmental Impact and Countermeasures section of this paper.

Attack Scenario #3: International Space Station

The International Space Station (ISS), shown in Figure 17, is the result of decades of work by several countries, primarily the United States, and cost many billions of dollars. A rogue state could strike a significant blow on US space assets if it were able to destroy or disable the ISS.

An attack on the ISS by a deadly minefield may stall manned spaceflight indefinitely and could possibly eliminate any justification for continuing to use the Space Shuttle.



Figure 17 International Space Station

Target Size

It can be seen in Figure 17 that the ISS “flies” around the earth in an upright “T” position. This means the ISS will be flying into the minefield in this same position. A crude estimation of the critical area of the ISS was made by multiplying the height of the habitable section of the ISS, 27.5 meters, by the width of the ISS components, 5 meters. This results in a cross-sectional area of approximately 140m^2 . Using the rule mentioned in the beginning of the Attack Scenario #1 section, the critical area was assumed to be 50% of the total habitable section area. This results in a critical target area of the ISS of 70m^2 .

The total target area of the ISS was calculated by adding the 140m^2 to the total ISS solar wing area of 892m^2 . This results in a total area in view of the minefield of 1032m^2 .¹¹

It should be mentioned that although the goal is to see the probability of striking a critical hit on the ISS, the solar wings and the Space Shuttle (when docked) will significantly increase the likelihood of the ISS being hit by the minefield. Although these hits outside the critical area may not destroy the station, the repeated hits may degrade the power and other systems to a point that keeping the ISS manned and in use may be impractical. In addition, repeated strikes to non-critical

systems of the station will cause a local debris cloud that will contribute to the debris problem.

Attack on the ISS

The ISS is located at an approximate altitude of 380 km at an inclination of 51.6 degrees. In order to maximize the relative velocities of the mines with respect to the ISS, the MDD is launched into a retrograde orbit which matches that of the ISS. This results in the relative velocities of the mines being roughly 15 km/s.

The MDD is deployed in this attack scenario to create a “shotgun blast” of particles which pose a serious threat to the ISS. Due to the lack of many spacecraft at 380 km in altitude, the minefield will pose a minor threat to other orbiting spacecraft which intersect the orbit of the minefield.

For the purposes of this study, it is assumed that the Delta IV Medium+ (5, 4) launch vehicle can lift approximately 50% of the payload into a retrograde orbit that it can lift into a polar orbit. This results in a payload capability of approximately 5000 kg. Therefore, it is possible to pack 25 million mines into the launch vehicle.

The MDD is detonated over the equator to result in a “ring” shape of mines focused on the target ISS orbit. The precession of periapse and line of nodes of the mines (relative to the station) is not a concern in this attack scenario. The minefield is deployed fairly low in the atmosphere which results in increased atmospheric drag. This causes the minefield to decay in orbit much faster than the previous two attack scenarios. Therefore, since the duration of the minefield is limited to days instead of years, the precessions are not a significant concern.

Minefield After 1 Day

Figure 18 shows the distribution of mines in orbit 1 day after the MDD was detonated over the equator.

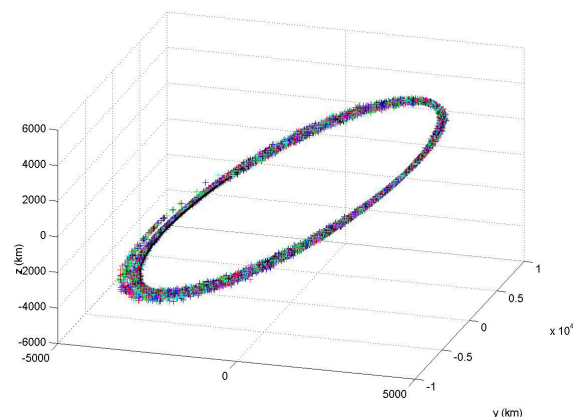


Figure 18 Minefield after 1 day

The black circle in Figure 18 shows the target orbit of the ISS. Figure 18 also shows that the mines have spread out within 1 day to completely fill the targeted ISS orbit. The various orbit altitudes of the mines after 1 day can be seen below in Figure 19.

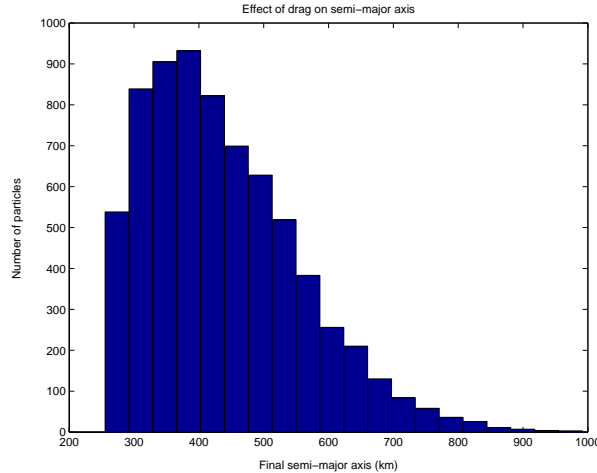


Figure 19 Semi-major axes of mines after 1 day

It can be seen in Figure 19 that the mines have spread out to a wide range of altitudes after the initial deployment from the MDD. However, one major factor in the movement of the mines through various altitudes is atmospheric drag. (See Equation 26) Even after 1 day, a significant portion of the minefield has reentered the atmosphere. In fact, roughly 29% of the mines have reentered the Earth’s atmosphere at this point.

The probability that the targeted International Space Station will suffer a hit during the first day of the deployment of the minefield is shown in Table 8 below.

Table 8 Probabilities of impact through 1 day

Type of Probability	Critical Area Impact Probability (%)	Total Area Impact Probability (%)
In Plane, 3-sigma STD Volume	9.2	85.5
In Plane, Total Volume	5.1	46.6
Out of Plane, 3-sigma STD Volume	0.1	0.9
Out of Plane, Total Volume	0.1	0.9

Table 8 shows the probability of impact in the critical and total ISS areas through the first day of the minefield deployment. Based on these probabilities, the ISS has a roughly 9% chance of suffering a critical hit within the first day of the deployment of the minefield. However, the probability of the ISS being hit anywhere by a mine is quite significant at 85.5%.

It is also seen in Table 8 that the out of plane probabilities are extremely low for this attack scenario. This is due to the fact that the minefield, although spread out through the ISS orbit, is tightly-packed together and decaying in orbit fairly rapidly. This means that satellites passing through the minefield orbit will “see” a small, concentrated area of mines as opposed to a larger, less concentrated mined region.

Minefield After 10 Days

Figure 20 shows the distribution of mines in orbit 10 days after the MDD has been detonated over the equator.

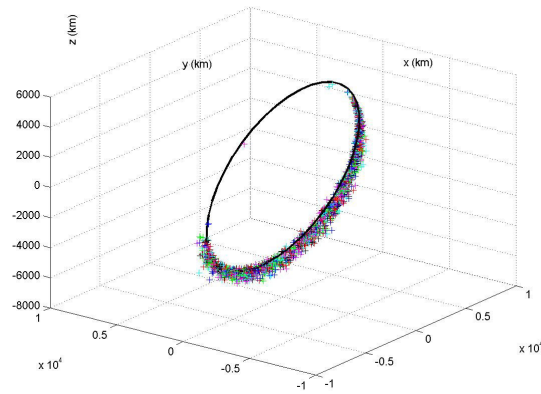


Figure 20 Minefield after 10 days

The black circle in Figure 20 shows the target orbit of the ISS. Figure 20 shows that after 10 days the minefield has become “bunched-up” on approximately half of the ISS orbit. The reason for this is that after 10 days, since approximately 85% of the mines have reentered Earth’s atmosphere (shown in Figure 21), the only remaining particles are those with high perigees. These “high perigee” particles were given a greater portion of energy in the detonation of the MDD that the rest of the mines. This caused these remaining 15% of the mines to remain in orbit with similar perigees for a longer time period. Since the orbits of these particles have similar perigees, they appear in Figure 20 to be somewhat bunched together in roughly half of the target orbit.

Figure 21 shows the how drag has effected the semi-major axes of the mines after 10 days in orbit.

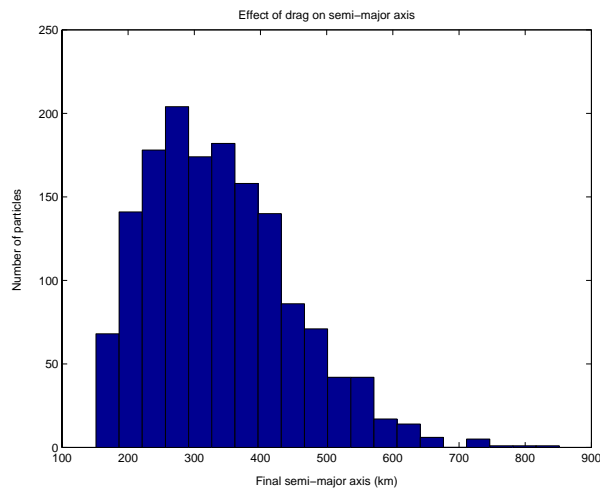


Figure 21 Semi-major axes of mines after 10 days

The altitudes of the mines are shown in Figure 21 to have been lowered due to atmospheric drag effects over 10 days in LEO. Many mines have reentered the Earth’s atmosphere by this point. In fact, nearly 85% of the mines have reentered Earth’s atmosphere after only 10 days in orbit. The mines in this attack scenario have a much shorter duration in orbit than the previous two attack scenarios.

The probability that the targeted International Space Station will suffer a hit during the first 10 days of the deployment of the minefield is shown in Table 9 below.

Table 9 Probabilities of impact through 10 days

Type of Probability	Critical Area Impact Probability (%)	Total Area Impact Probability (%)
In Plane, 3-sigma STD Volume	19.2	99.0
In Plane, Total Volume	11.0	88.7
Out of Plane, 3-sigma STD Volume	0.2	1.0
Out of Plane, Total Volume	0.2	1.0

Table 9 shows the probability of impact in the critical and total ISS areas through the first 10 days of the minefield deployment. Based on these probabilities, the ISS has a roughly 19% chance of suffering a critical hit within the first 10 days of the deployment of the minefield. Although this chance of a critical impact may seem small, the total cross-sectional area of the ISS has a roughly 99.0% chance of being struck by a

mine within the first 10 days of the deployment of the minefield. This means the minefield is almost guaranteed to hit the ISS within 10 days.

It is also seen in Table 9 that the out of plane probabilities are still extremely low for this attack scenario. This occurs for the same reason explained in the previous section (minefield after 1 day).

Minefield Effectiveness Over Time

Figure 22 below displays the daily probability of a critical strike on the ISS over time. This means that each probability in the plot at a given day was calculated through that entire day. Please note that the y-axis values are decimal probabilities, not percentages.

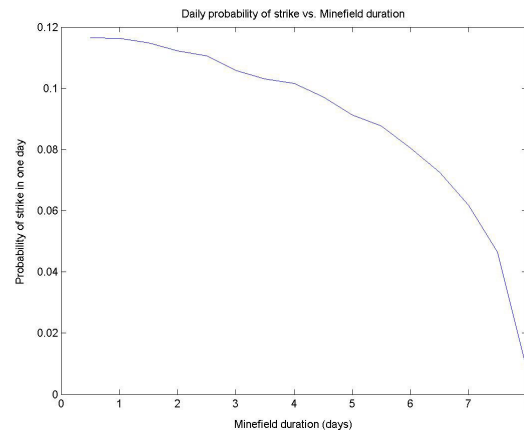


Figure 22 Daily probability of critical impact over time

Figure 22 clearly shows that the minefield used to attack the ISS will only present a significant threat until approximately 8 days in orbit. By the 8th day in orbit, the minefield’s daily probability of striking the space station has decreased dramatically.

Attack Scenario 3: Environmental Impact and Countermeasures

The International Space Station, if it suffered an impact at a critical area such as an inhabited module, would most likely need to be abandoned until repairs could be made. However, if repeated critical strikes were made on the ISS, it may be forced to be abandoned forever. The cost may become too great to repair and protect the ISS from minefields such as those discussed in this paper.

Being 6mm in diameter, the particles deployed from the MDD are not able to be tracked from the ground. This prevents the ISS from being maneuvered out of the way of the approaching debris field. This removes one option of defense from the ISS.

The ISS designers have taken significant steps to protect the crew and sensitive components from orbital debris impacts. “For example, the ISS has a shield that will protect it from debris smaller than 1cm across by exploding them into even tinier particles, which some say could actually increase the debris problem...pieces between 1 and 10cm will generate a shower, several of which could penetrate the hull.”¹² The type of shield being referred to in the previous quote is a Whipple-type shield. The basic design of the shield is shown below in Figure 23.

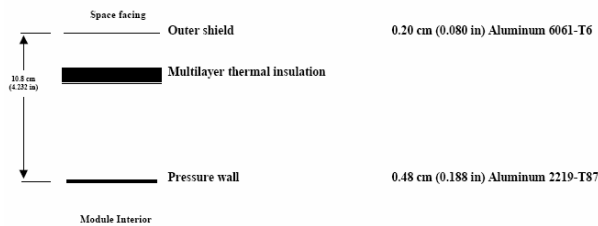


Figure 23 Example Whipple shield¹³

The Whipple shield works by causing impacting orbital debris particles to break apart at the outer, thinner wall into much smaller pieces which then impact the thicker, inner hull over a larger area, thus spreading out the energy of impact.

Although the earlier quote mentions the protection for particles up to 1cm across, an AIAA paper describing the survivability of the ISS from space debris has a different view. A figure in the paper shows that the survivability of the ISS from a direct impact from an orbital debris particle traveling at 15 km/s is only for particles less than 5.5cm in diameter.¹⁴ Therefore, the 6mm diameter mines in this study would likely be able to penetrate the ISS.

In addition, the assumption made for the particles is that they are made out of aluminum. Also, the particles most likely to impact the ISS from other debris sources are probably irregularly-shaped objects such as paint flakes. The 6mm diameter mines used in this study have a density similar to that of aluminum but are in the shape of solid spheres of material. This shape may help the particles penetrate the Whipple-type shield more easily than an irregularly-shaped debris object.

In addition, NASA has expressed serious concern about debris objects like the mines used in this study. NASA has shown in a technical paper about the impact of orbital debris on the Space Shuttle that particles 5mm and larger could penetrate all critical portions of the Shuttle including the crew cabin.¹⁵ If objects such as the ones used for the minefield in this study can penetrate the crew cabin of the Space Shuttle, it may be likely they can penetrate the crew cabin of the International Space Station.

Other Countermeasures

The Whipple-type shield could be improved to include layers of KevlarTM fabric and/or NextelTM foam cladding. The addition of TeflonTM may also improve the effectiveness of the shielding against orbital debris.¹⁶

Other Environmental Impacts

A major potential environmental impact of an intentional minefield is the creation of a self-propagating minefield. For every collision that takes place between a mine particle and a target object, potentially hundreds or thousands of other orbiting debris particles could be created. These particles, in turn, could impact other objects and continue the self-propagating cycle of orbital debris impacts. This effect was not analyzed in this study, but can only contribute to the effectiveness of the minefield.

Another potential major environmental impact of this minefield is the potential of the forced abandonment of the ISS. If, for some reason, the ISS is abandoned and reenters the Earth uncontrollably, it could cause damage on the surface up to and including loss of life. Just as Skylab reentered years ago with large pieces crash-landing in Australia, a much larger ISS could break apart into several large pieces which may cause damage somewhere on Earth.

Software Module

Requirements

In order to “study the threat of a rogue state ‘mining’ low-Earth orbit (LEO),” a software tool was written to analyze and quantify the threat posed by several different scenarios. Thus, the following requirements were specified for the software:

- Allow the user to input a ‘reference’ minefield orbit
- Allow the user to describe the mines and minefield in a useful way
- Allow the user to specify the nature of the ‘target’ spacecraft
- Generate from the input a reasonable model of the minefield
- Use this model to quantify the ‘threat’ to LEO spacecraft in some way
- Visualize the minefield

The Matlab module that was created to address these requirements is presented in full in Appendix A, and a description of the code follows presently.

Description of Code

This section represents a description of the code used to analyze this problem, complete with required inputs, sample outputs, applicable formula, and assumptions.

The first part of this description may also be considered a users guide for the tool, as the whole program can be manipulated by adjusting the initial parameters.

Constants

Several values were assumed constant and referenced in the code where appropriate. These were the gravitational parameter μ , the radius of the Earth, R_e , and the J_2 term for the Earth, J_2 . The values used in the code are presented in Table 10. All of these parameters can be easily updated in the software as required.

Table 10 Program constants

Constant	Value
μ (m ³ /s ²)	3.986e14
R_e (m)	6.38e6
J_2	0.00108263

Inputs

As mentioned in the software requirements, it is necessary to allow the user to adjust various parameters of the mines, the minefield, and the target spacecraft. The following list is a description of the available setup parameters with their required units.

$v_disperse$ (ft/s): This is the initial dispersion velocity of the minefield particles. For this model, it is assumed that the mines are arranged spherically around an explosive mechanism, and that the ΔV is normally distributed in each axis with mean zero and standard deviation of $v_disperse$. Thus, the maximum ΔV per axis is $3*v_disperse$ for 99.73 percent of the particles (3-sigma deviation). This value is input in English units so that easy analogy might be made to typical terrestrial projectiles, such as bullets. The initial dispersion velocity is converted to metric units before use.

alt (km): This is the initial altitude of the minefield orbit, when it is assumed to be circular. If orbital elements or exact position and velocity vectors are given for the minefield orbit initial condition, then this value is overridden. This value is converted to meters before use.

$tfinal$ (days): This is the ending time of the simulation. All results are calculated and presented after the minefield has been propagated to $tfinal$. This value is converted to seconds before use.

$objects$: This is the number of mines to propagate for a given run. The simulator then calculates a random initial velocity for each object (see $v_disperse$ above) and performs a Monte-Carlo analysis using this many trials. The user should be careful in choosing extremely

large values of $objects$, for this directly impacts the run time of the simulation. As an example, 50,000 objects can be computed on a typical desktop computer in a few minutes.

$s_objects$: This is the number of mines that can be packed into the launch vehicle. The simulator performs a Monte-Carlo analysis on $objects$ number of trials, and then extrapolates the results to $s_objects$. The assumption is that a proportional number of the actual mines will re-enter the atmosphere as in the restricted case, and that the actual minefield will occupy a similar volume of space as the restricted case. Thus, it is not necessary to run the simulation for the full number of projectiles in the launch vehicle, only a representative number. This is a reasonable assumption for large values of objects. For example, if the code is run for 10,000 objects, and then 3-sigma boundaries were drawn to enclose the resulting volume, statistically one would expect only 135,000 objects to fall outside of those bounds for a 50 million projectile run. While this seems like a large number, it only represents a 0.2 percent error in the resulting spatial density of the cloud.

dp (m): This is the diameter of the mines, assumed to be spherical.

Cd : This is the coefficient of drag on the mines, generally assumed to be 2.2 for a sphere, unless actual experimental drag measurement data is available.¹⁷

mp (kg): This is the mass of the individual mines.

ρ (kg/m³): This is the density of the atmosphere in the vicinity of the minefield, referenced from a table (see SMAD¹⁸, inside back cover). Since the simulator is not capable of adjusting the density as the altitude of the particles decreases due to drag, typically a conservative value is used. For example, if the mines are to be injected into an 800 km orbit, a value of density for 600 km might be used, thus assuring the user that all mines remaining above 600 km at the end of the run would have survived at least that long (but probably much longer).

Ac (m²): This is the critical cross-sectional area for collision for the target spacecraft. The value Ac represents a conservative estimate of the planar area of the target vehicle that is vulnerable to catastrophic failure if struck by a piece of debris. In general, solar arrays and other appendages are not considered in this area, and even the main planar area is cut by a large fraction. This is to help distinguish critical components of the craft such as fuel tanks, attitude control components, batteries, and computers, from less critical components such as structural members. Obviously, this assumption neglects any secondary consequences

of a non-critical strike (which can only be bad), since the focus of this paper is on the potential of the minefield to disable spacecraft in LEO.

t_mission (days): This is a separate time from the simulation time, representing the time period in which the user wants to know the probability of strike. For example, if *t_final* was set to 30 days, and *t_mission* was set to 10 days, the equivalent question would be: “What is the probability of a mine striking the target, if the target orbited for 10 days in the minefield that results after 30 days of dispersal?” The problem with this setup is immediately obvious: during the *t_mission* time, the minefield dispersion is changing, and the orbits are decaying. However, for small *t_mission*, or high altitude orbits (small decrease in altitude over time), this is an acceptable approximation.

a_target (km): This is the altitude of the target satellite. The parameter *a_target* is used to calculate how long the target spacecraft is in the debris field when calculating the probability of strike for satellites that are not in the debris plane. Before use it is converted to meters and added to the radius of the Earth, thus representing a true radius to the target satellite.

r_cutoff (km): This is the altitude at which the mines are assumed to have re-entered the atmosphere. Since the rate of orbital decay is extremely high below 150 km, and there are few targets at those low altitudes (if any), this value is typically set near 150 to 200 km.

xo (m, m/s): This is a vector of initial conditions for the minefield orbit. It can be generated in several ways, as will be presented below. The first three terms are the initial radius vector to the point of detonation, in Earth-Centered Inertial (ECI) coordinates, and the last three terms are the initial velocity vector also in ECI.

Activations

Several switches have been provided for the user to customize the output and performance of the program. A description of these functions follows:

make_plots: This switch allows the user to enable or disable all of the graphical output of the code. This might be desirable if running multiple cases in a series to fill a table of probabilities.

plot_bounds: This switch turns the visualization of the worst-case boundaries off and on (see Figures 6 - 8).

use_J2: Turning this switch off makes the simulation behave as though the Earth were a uniform sphere.

use_drag: Turning this switch off disables the drag calculations in the simulation.

use_keep_list: This option specifies whether the simulation should remove particles that have re-entered or not. If this switch is enabled, mines that fall below *r_cutoff* are removed from the plot, and the spatial density calculation is scaled appropriately.

disk_volume: This switch tells the software to use a disk to approximate the volume of the minefield (see description below).

sshell_volume: This switch tells the software to use a spherical shell to approximate the volume of the minefield (see below). If both *disk_volume* and *sshell_volume* are enabled, the spherical shell technique overrides.

Operation and Equations

The following section details the operation of the software tool and presents the necessary theory. The description is presented in a similar order to the code, so the user can compare the implementation if desired. The software is well documented and included in Appendix A.

The operation of the software analysis tool is comprised in bulk by the *debris_pert.m* file, written in Matlab. The code begins by initializing the values above, and then converts all non-standard units into fundamental units. The code then creates the initial condition vector for the minefield, *xo*, either from user-defined orbital elements or a simple description of radius and position (for example, a radius vector of $\{r, 0, 0\}$ and a velocity vector of $\{0, 0, v_c\}$ where v_c is the circular speed at radius r). The bulk of the simulation then begins.

The idea of the simulation is to propagate the orbits of the individual mines through some time (*t_final*), and then use the resulting distribution to determine the spatial density of the minefield and thus the probability of strike. Each individual mine is given a normally distributed random ΔV at time zero, to simulate the variation of initial velocities of the particles when dispersed by explosion. Each of these new orbits is then simulated in turn.

One relatively easy and computationally cheap way to propagate an orbit, when only the endpoint is desired, is to use orbital elements. Many variations on the standard orbital elements are common, but one useful set is: semi-major axis, eccentricity, inclination, true anomaly, longitude of the ascending node, and argument of periapse. These are symbolized as a , e , i , v , Ω , and ω , respectively. A series of relatively simple calculations will yield all six orbital elements from the position and velocity vectors of a spacecraft, as follows:

$$\vec{h} = \vec{r} \times \vec{v} \quad (3)$$

$$\vec{N} = \hat{z} \times \vec{h} \quad (4)$$

$$p = \frac{h^2}{\mu} \quad (5)$$

$$a = -\frac{1}{\left(\frac{v^2}{\mu} - \frac{2}{r}\right)} \quad (6)$$

$$\vec{e} = \frac{1}{\mu} \left(v^2 - \frac{\mu}{r} \right) \hat{r} - (\vec{r} \cdot \vec{v}) \vec{v} \quad (7)$$

$$i = \cos^{-1} \left(\frac{\hat{z} \cdot \vec{h}}{h} \right) \quad (8)$$

$$\Omega = \cos^{-1} \left(\frac{\hat{x} \cdot \vec{N}}{N} \right) \quad (9)$$

$$\omega = \cos^{-1} \left(\frac{\vec{e} \cdot \vec{N}}{eN} \right) \quad (10)$$

$$\nu = \cos^{-1} \left(\frac{\vec{e} \cdot \vec{r}}{er} \right) \quad (11)$$

Here all quantities not indicated with an over-arrow are scalar quantities. The position and velocity vectors \mathbf{r} and \mathbf{v} are given, the gravitational parameter μ is given, \hat{x} and \hat{z} are the unit vectors in the x and z direction, \mathbf{h} is the angular momentum vector, \mathbf{N} is the vector direction of the orbit node, p is the orbit parameter, and a , e , i , ν , Ω , and ω are defined above. This conversion from position and velocity vectors to orbital elements is done in the software by the *rv2orbel.m* function, included in Appendix A. Note also that there are several sign checks that must be performed due to the inverse cosines, and these checks can be examined in the attached code. The software also makes provisions for circular and equatorial orbits, where some of these parameters are ill-defined.

Once the orbital elements have been calculated, the orbit can be easily propagated. In the absence of disturbing forces, all of the orbital elements remain constant except for the true anomaly. The true anomaly can be propagated relatively easily by converting it to the eccentric anomaly, E , and then using Kepler's Equation as follows¹⁹:

$$E = \cos^{-1} \left(\frac{e + \cos(\nu)}{1 + e \cos(\nu)} \right) \quad (12)$$

$$M = E - e \sin(E) \quad (13)$$

$$n = \sqrt{\frac{\mu}{a^3}} \quad (14)$$

$$M_{new} = M_{old} + nt \quad (15)$$

Here M is the mean anomaly, n is the mean motion of the spacecraft, and t is the time to propagate to (from epoch of zero). Having propagated the mean anomaly forward, Kepler's Equation (13) can be solved again, but now for the eccentric anomaly, which can then be converted into the true anomaly ν . Kepler's Equation is one of the most studied equations of all time, yet still there is no exact analytic solution for E as a function of M . Fortunately, Matlab can solve it numerically, and the function *kepler.m* was created for precisely that purpose. Then to get the true anomaly:

$$\nu = \cos^{-1} \left(\frac{\cos(E) - e}{1 - e \cos(E)} \right) \quad (16)$$

Again a quadrant check must be performed as indicated in the software source code. Once the new true anomaly has been calculated, it is a relatively simple task to obtain the position and velocity vectors from the new orbital elements. The necessary equations, presented by Battin,²⁰ are as follows:

$$p = a(1 - e^2) \quad (17)$$

$$r = \frac{p}{1 + e \cos \nu} \quad (18)$$

$$h = \sqrt{p\mu} \quad (19)$$

$$\theta = \omega + \nu \quad (20)$$

$$\vec{r} = r [(\cos \Omega \cos \theta - \sin \Omega \cos \theta \cos i), \\ (\sin \Omega \cos \theta + \cos \Omega \sin \theta \cos i), \\ (\sin \theta \sin i)] \quad (21)$$

$$\begin{aligned} \vec{v} = & -\frac{\mu}{h} [(\cos \Omega(\sin \theta + e \sin \omega) + \\ & \sin \Omega(\cos \theta + e \cos \omega) \cos i), \\ & (\sin \Omega(\sin \theta + e \sin \omega) - \\ & \cos \Omega(\cos \theta + e \cos \omega) \cos i), \\ & -(\cos \theta + e \cos \omega) \sin i] \end{aligned} \quad (22)$$

These equations are implemented in the function *orbel2rv.m*, included in Appendix A. The result of this formulation, when applied repeatedly to 10,000 individual particles, is shown in Figure 24. In this example, the initial path is a polar orbit, the explosion takes place as the MDD crosses the equator, and the particles were propagated forward a year.

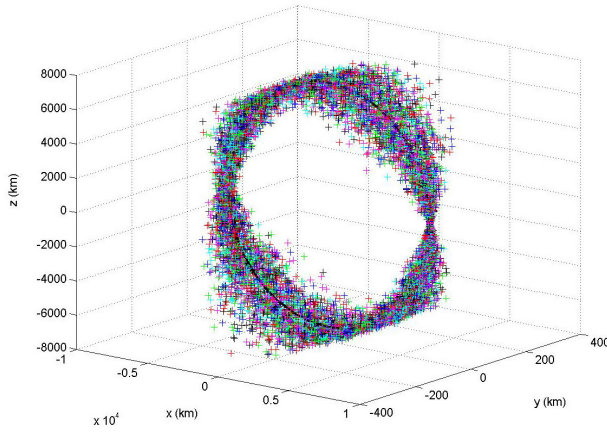


Figure 24 Result of 10,000 objects after 1 year, no drag or J2

It is interesting to note the “hourglass” shape of the resulting distribution, where the well-defined crossing indicates the point of detonation. Because in this run the Earth was assumed to be spherical, the point of detonation is the periapee of every orbit, and it remains in the same place over time. One should also be careful to observe the scales on this plot. The y-axis is markedly spread out compared to the x-axis and z-axis, giving the illusion of a thick band; in reality, however, this figure represents a rather thin ring (on an orbital scale).

It is quickly obvious from the compactness of the perigee in the plot above that a spherical Earth has been assumed. Using the orbital elements, however, it is easy to account for the most significant non-spherical Earth term, the J_2 effect. As mentioned above, in the absence of outside forces, the only orbital element that must change in time is the true anomaly. If J_2 is used, however, there are variations with time in the longitude of the ascending node and the argument of periapee (and also the mean motion, though not an orbital

element in this code). These variations can be expressed as follows, as presented by Chobotov²¹:

$$\bar{n} = \sqrt{\frac{\mu}{a^3}} \cdot \left(1 + \frac{3}{2} \frac{J_2 \cdot r_e^2}{p^2} \cdot (1 - \frac{3}{2} \sin^2 i) \cdot \sqrt{1 - e^2} \right) \quad (23)$$

$$\dot{\Omega} = -\frac{3}{2} \frac{J_2 \cdot r_e^2}{p^2} \bar{n} \cos i \quad (24)$$

$$\dot{\omega} = \frac{3}{2} \frac{J_2 \cdot r_e^2}{p^2} \bar{n} (2 - \frac{5}{2} \sin^2 i) \quad (25)$$

Here the J_2 constant is as defined at the top of this section, and $\dot{\Omega}$ and $\dot{\omega}$ are the time rate of change of the longitude of the ascending node and the argument of periapee, respectively. The equations above have been implemented in the code to augment the basic strategy outlined previously. The following figure is an example of this implementation on 10,000 particles starting out in an equatorial orbit and propagated for a year.

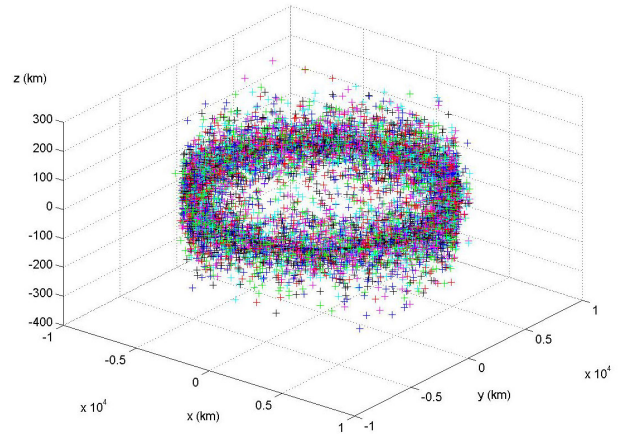


Figure 25 Result of 10,000 objects after 1 year, no drag

The distinction between this result and the “no J_2 ” result is readily apparent. Due to the precession of the argument of periapee and the longitude of the ascending node, now there is no hourglass structure or evidence of the point of the explosion. The disk of debris is now quite uniform.

This model is more complete than the last; however it is still missing a key component. The spherical particles selected have a relatively small ballistic coefficient and so it is expected that they will lose a lot of energy to drag. Like J_2 , drag is also easy to implement using the variational orbital element method. The drag force

acting on the mines has an effect on two orbital elements: eccentricity and semi-major axis. Because the drag force operates more strongly at perigee than apogee for elliptical orbits, it has a tendency to circularize elliptical orbits until the eccentricity is zero. For orbits that are nearly circular to begin with, the only effect is to reduce the semi-major axis with time. Chobotov²² presents this rate as follows:

$$\dot{a} = -\sqrt{\mu a} \rho B \quad (26)$$

Here r is the density of the atmosphere at the particle's altitude and B is the ballistic coefficient, defined by Chobotov as:

$$B = C_D A / M \quad (27)$$

Here C_D is the coefficient of drag on the particle (2.2 for a sphere), A is the cross-sectional area of the particle, and M is the particle's mass. Note that the units of this "ballistic coefficient" are m^2/kg , which is contrary to the ballistic coefficient defined by many other sources (but is the correct definition for the equation above).

Implementing this variational parameter makes the model complete; that is, it is reasonably accurate for the present purposes. A future study might include solar radiation pressure as an effect on the particle, however since the direction of this force changes as the Earth moves around the sun, the implementation is significantly more complex. Similarly, a future model might use a density model that accounts for the changing density over time (as the semi-major axis shrinks).

The figures presented the first sections of this paper (for example, Figures 3 and 9) all use the full model including J_2 and drag effects, so the reader may see sample results on those earlier pages.

After computing the final location of all of the objects required, the *debris_pert.m* code continues to analyze the resulting data. First, the radius of perigee, r_p , for each particle is determined, where:

$$r_p = a(1 - e) \quad (28)$$

The code then compares the radii of perigee to the minimum allowable altitude as defined by the user, and flags every failed particle. The lost particles are not plotted and are not counted when calculating the density (that is, the density goes down).

If desired, the software will then generate a number of plots for the user. Each plot is useful in its own way. The primary plot is the three-dimensional visualization of the endpoints as shown in several figures, such as Figures 3 and 9. In addition, histograms can be created from the orbital elements, showing trends among the mines. For example, Figures 26 and 27 below show the distribution of inclination angle and eccentricity for the particles from the "no drag" example above. Similar plots can be generated for all of the orbital elements.

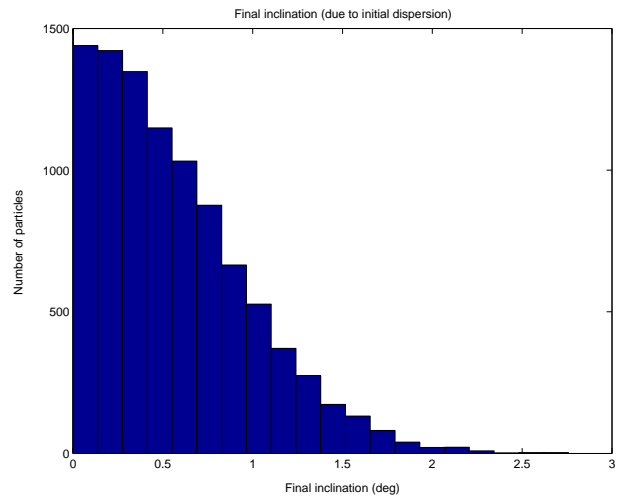


Figure 26 Final inclinations of 10,000 objects after 1 year, no drag

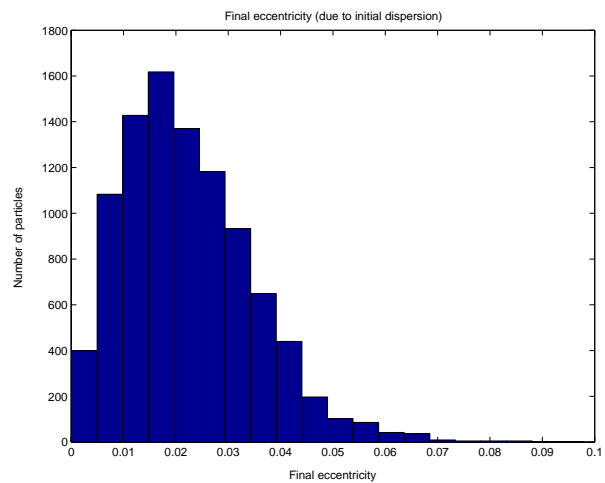


Figure 27 Final eccentricities of 10,000 objects after 1 year, no drag

Probability of Strike

After creating the desired plots, the code then analyzes the data to estimate the spatial density of the minefield, in order to calculate the probability of strike. This is

done in several ways, one of which is very conservative, and another which is more realistic but doesn't contain every particle.

Looking at the data, it is apparent that the generated minefields take on two major shapes: disks and spherical shells. Disks can be generated, for example, by initial equatorial orbits or polar orbits with the explosion at the pole. Spherical shells can be generated using a polar orbit with the detonation at the equator. Thus, knowing the shape that the resulting minefield will take, the volume can be estimated by appropriately sizing the sphere or disk.

One obvious way to size the sphere and disk is to find the pair of radii that enclose every particle in the run. That is, for the spherical shell, the outer radius would be the largest radius of apogee of any particle, and the inner radius would be the smallest radius of perigee of any particle. This would also work for the disk, however the thickness of the disk is also required to fully define the volume. To contain every object, the thickness of the disk needs to be the maximum out-of-plane component of any mine, which can be calculated as the radius of perigee times the sine of the inclination (or, more precisely, the change in inclination from the reference orbit). This method generates a very conservative volume that encloses every particle, and when the number of surviving particles is divided by this result, the answer is an estimate for the spatial density of the minefield.

Looking at the red lines on Figure 7 (calculated in this manner), it is obvious that this estimate is entirely too conservative. A more realistic result was arrived at by, instead of finding the maximum radius of apogee and minimum radius of perigee, finding the radii that enclosed 99.73 percent of all mines. That is, finding the 3-sigma values of r_a and r_p to enclose the disk or sphere. The result of that approach is indicated by the blue lines on Figure 7, and is clearly a more representative volume.

The probability of a spacecraft being struck by a piece of debris, in a debris cloud with density ρ , is given by Chobotov²³ as:

$$P = 1 - e^{-\rho v_r A_c \Delta t} \quad (29)$$

Here v_r is the relative velocity, A_c is the cross-sectional area for collision, and Δt is the mission time. In this software tool, it is assumed that the debris cloud is launched into an orbit that is retrograde with respect to the target. Thus, the relative velocity is roughly twice the circular speed of the target, for a target that is in the plane of the debris field. Since it is not possible that all target spacecraft will be in the plane of the debris field,

but that many (if not most) will cross the field only in two places per revolution, an out-of-plane probability is also calculated. For a worst case, it is assumed that the secondary target has a crossing orbit that is normal to the minefield. Thus, the relative velocity is the orbital velocity times the square root of two, and the percentage of the target vehicle's orbit spent in the minefield is only twice the thickness of the disk over the circumference of the orbit. The out-of-plane probability is thus recalculated in this fashion, giving an estimate of the probability of strike for an out-of-plane spacecraft. In this way, the numbers presented in the tables above were calculated, and a quantitative measure of "the threat of a rogue state 'mining' low-Earth orbit (LEO)" was obtained.

Orbit Survey

One task that was required for this project was to understand what objects were in orbit, and where they were. This information proved very difficult to find; there are few current surveys available that give the general trend of what is in orbit (altitude, semi-major axis, etc). Much information is available in the form of two-line element (TLE) sets, however, so a module was written to dissect the TLE data and create useful representations from them. This program is called *parse_tle.m*, and is included in the Appendix.

The simplest way to obtain current TLE sets was found to be the Satellite Toolkit (STK). STK has a feature that allows it to update its database of known spacecraft from the internet, and then this current data can be sorted and saved to a file of TLE sets. The *parse_tle.m* code reads this file line by line and extracts the desired orbital elements for each satellite, namely: semi-major axis, eccentricity, and inclination. Many of these parameters are in odd units or have decimal places assumed, so the code converts each element accordingly. The longitude of the ascending node can also be extracted, however since the epoch of each TLE set is different, this data is largely meaningless without transformations in a rotating coordinate frame. After parsing the text file to extract a , e , and i , this module then plots histograms of the data, indicating trends in current spacecraft orbits and allowing the selection of potential minefield orbits. Sample output from this code can be seen in Figures 1 and 2.

Conclusion

The launch and deployment of the MDD system could be accomplished by a rogue nation for approximately 100 million dollars. This cost includes the launch vehicle, mines, explosives, and MDD structure. Since the launch vehicle is by far the most expensive item in the list, the cost of the other components is insignificant by comparison.

It has been shown that significant damage can be done by implementing such a system to attack space assets. Attack scenario #1 showed a significant long-term effect on the safety of some LEO orbits. However, constellations such as Iridium would likely be able to continue to function since the constellation has many different satellites in different polar orbits. The constellation also has many on-orbit spares.

Attack scenario #2 showed that nearly all LEO orbits could be attacked by the minefield as well. Although the probabilities of being impacted were somewhat small, these numbers were for all spacecraft in the minefield. This means there is a significant potential of a great number of satellites being critically damaged by the minefield for this type of attack.

The results from attack scenario #3 show that the ISS can be struck from such a minefield. Although it is much more likely that a non-critical system will be impacted by a mine, this hazard may require additional shielding or possibly the abandonment of the space station. The cost to protect the ISS may end up dooming the station. Already, “the cost of ‘armor-plating’ the ISS against man-made rubbish has added at least \$5 billion to”²⁴ the cost of the station. If additional shielding is required once faced with the threat of this rogue nation’s minefield, the nations constructing the ISS may not want or have the cash to pay the bill.

The danger of the minefield proposed in this paper, although having the potential of causing some damage to US space assets, could not create the sort of damage to US space assets that would give a rogue nation a significant military advantage. The main US communications satellites, such as Milstar, are located in geosynchronous orbits and are out of the scope of this proposed minefield. Therefore, the US government need not consider the threat from such a weapon as the MDD minefield a serious threat from foreign countries.

Future Work

One major topic for future work could be the investigation of the ability of such a minefield to self-propagate. The long-term effects of this self-propagation could be investigated. The minefield may actually pose more of a danger than realized in this paper.

Other types of mines could be investigated as well. Different sizes, shapes, and materials could be studied for their effectiveness against targets in space.

Improved analysis of the explosion dynamics would lead to more accurate initial conditions for the mines and a more robust estimate of the mass of the explosive. In addition, a more detailed design of the explosion

would lead to necessary design constraints on the MDD container itself.

Improved software models that account for the changing density and solar radiation pressure could be included in the analysis tools.

Other targets beyond those investigated in this paper could be studied as possible targets for the MDD. Geosynchronous satellites, much more expensive and powerful than satellites in LEO, may be good targets to attack with the MDD. Serious damage to US space assets could be done by destroying GEO communications satellites.

Finally, the use of multiple MDDs could be investigated to see how several MDDs could be used in a coordinated fashion to design an effective attack strategy against a specific target.

Appendix A

debris_pert.m

```
clear all

#####
% Constants

global MU;
global re;
colorwheel = 'rgbkmc';
MU = 3.986e14;      % [m^3/s^2], this is for the ****Earth****
re = 6.38e6;       % [m], ****Earth**** radius
J2 = 0.00108263;  % J2 term at the ****Earth****

#####
% Here are the setup parameters, note units. Many are in odd units
%   for ease of intuitive thinking

v_disperse = 300;      % [ft/s] initial spherical dispersion velocity (this is 1 sigma!!!)
alt = 780;            % [km] initial altitude of explosion
tfinal = 365;         % [days] duration of sim
objects = 10000;      % [#] number of objects in canister
s_objects = (50e6);   % number of objects to assume in canister w/ same results as above
dp = 6e-3;           % diameter of the projectile
A = (1/4)*pi*(dp^2); % planar area of projectile in m^2
Cd = 2.2;            % coefficient of drag for the projectile
mp = .2e-3;          % mass of the projectile (kg)
B = Cd*A/mp;         % [m^2/kg] ballistic coefficient
rho = 4.89e-13;      % atmospheric density, make sure this matches altitude given above
                    % (now using density for 600km at alt of 800km
                    %   for worst-case) (800 km: 4.39e-14)
                    % density for [350m]

% rho = 1.66e-11;
% Ac = 1032;
% Ac = 70;           % [m^2] critical cross section for collision for target spacecraft
                    % (ISS)
Ac = 1.29;          % [m^2] critical cross section for collision for target spacecraft
t_mission = 30;     % [days] duration of the mission (probability of getting struck in this
                    % time)
a_target = 780;     % [km] semi-major axis of target satellite
r_cutoff = 200;     % [km] cutoff altitude (radius of perigee) below which projectiles are
                    % assumed to have re-entered

#####
% Here are some switches for program activations (1=true)

make_plots = 1;
plot_bounds = 1;
use_J2 = 1;
use_drag = 1;
use_keep_list = 1;
disk_volume = 1;    % calculate probabilities using the disk approach for volume
sshell_volume = 0; % calculate probabilities using the spherical shell approach for
                    % volume

#####
% Now convert the units to standard SI if required

v_disperse = v_disperse/3.28; % [m/s] (3.28 ft/m)
r = re + alt*1000;           % [m], this is now radius, not altitude
r_cutoff = re + r_cutoff*1000; % [m] now this is truly a radius of cutoff
a_target = a_target*1000 + re; % [m] semi-major axis of target satellite
tfinal = tfinal*24*60*60;   % [s]
t_mission = t_mission*24*3600; % [s]

#####
% Calculate initial conditions of bomb and make IC vector
% NOTE: this doesn't have to be circular, but is an easy way to get IC's

% [ri, vi] = orbel2rv(380e3+re, .000528, 51.6295*pi/180, 166.9733*pi/180, 288.4644*pi/180,
230.0767*pi/180, MU);
% vc = sqrt(MU/(380e3+re));
% xo = [ri; vi];
vc = sqrt(MU/r);
xo = [r 0 0 0 vc 0]';
V_rel = 2*vc; % assume projectiles are travelling in opposite direction, same plane

#####
% Propagate the trajectories and work on the switches above
```

```

if use_J2 == 0
    J2=0;
end

if use_drag == 0
    B=0;
end

for j=1:objects
    v_rand = v_disperse*randn(3,1); % get the random component of the velocity
    x01 = x0 + [0; 0; 0; v_rand]; % build the IC vector
    [a, e, i, nu, node, omega] = rv2orbel(x01(1:3)', x01(4:6)', MU); % get the orbital elements
    from (r,v)

    Ea = acos((e+cos(nu))/(1+e*cos(nu)));
    Ma = Ea - e*sin(Ea); % calculate the mean anomaly
    p = a*(1 - e^2); % calculate the orbit parameter

    n = sqrt(MU/a^3)*(1 + (3/2)*((J2*re^2)/(p^2))*(1 - (3/2)*sin(i)^2)*sqrt(1 - e^2)); % J2
    perturbed mean motion
    dNode = (-3/2)*((J2*re^2)/(p^2))*n*cos(i); % J2 perturbed longitude of ascending node
    domega = (3/2)*((J2*re^2)/(p^2))*n*(2 - (5/2)*sin(i)^2); % J2 perturbed argument of
    periapse
    da = -n*(a^2)*rho*B; % drag perturbed semi-major axis (assumes constant drag
    even with changing alt!) % NOTE: drag eq. assumes near circular, otherwise e
    would change also!!!

    Ma = Ma + n*tfinal; % advance the mean anomaly to the new time
    node = node + dNode*tfinal; % advance node to the new time, only changes if J2 on
    omega = omega + domega*tfinal; % advance omega to the new time, only changes if J2 on
    a = a + da*tfinal; % advance a to the new time, only changes if drag is on

    global e_in M_in;
    e_in = e;
    M_in = Ma;

    Ea=fzero('kepler',Ma); % solve kepler's equation for the EA at the new time

    nu = acos((cos(Ea)-e)/(1-e*cos(Ea))); % recalculate the true anomaly
    if Ea > pi
        nu = 2*pi - nu; % sign check for the arccos
    end

    [r_new, v_new] = orbel2rv(a, e, i, nu, node, omega, MU); % get (r,v) back from the orbital
    elements

    data(j,:)=[r_new(1) r_new(2) r_new(3)];
    stat_data(j,:)=[a e i mod(nu,2*pi) mod(node,2*pi) mod(omega,2*pi)];
    if (mod(j,100)==0)
        j
    end
end

rp = stat_data(:,1).*(1 - stat_data(:,2));
if (use_keep_list == 1)
    keep_list = find(r_cutoff < rp);
else
    keep_list = 1:objects;
end
lost_count = objects - length(keep_list)

#####
% Do all the plotting if desired

if make_plots == 1

    figure
    hold on
    for j=1:length(keep_list)
        plot3(data(keep_list(j),1)/1000, data(keep_list(j),2)/1000, data(keep_list(j),3)/1000,
        [colorwheel(mod(j,6)+1)'+']);
    end
    grid on

    % plot the reference orbit, must advance this due to J2 also
    global MU_in;
    MU_in=MU;

```

```

[a, e, i, nu, node, omega] = rv2orbel(xo(1:3)',xo(4:6)',MU); % get the orbital elements
from (r,v)
Ea = acos((e+cos(nu))/(1+e*cos(nu)));
Ma = Ea - e*sin(Ea); % calculate the mean anomaly
p = a*(1 - e^2); % calculate the orbit parameter
n = sqrt(MU/a^3)*(1 + (3/2)*((J2*re^2)/(p^2))*(1 - (3/2)*sin(i)^2)*sqrt(1 - e^2)); % J2
perturbed mean motion
dNode = (-3/2)*((J2*re^2)/(p^2))*n*cos(i); % J2 perturbed longitude of ascending node
domega = (3/2)*((J2*re^2)/(p^2))*n*(2 - (5/2)*sin(i)^2); % J2 perturbed argument of
periapse
Ma = Ma + n*tfinal; % advance the mean anomaly to the new time
node = node + dNode*tfinal; % advance node to the new time, only changes if J2 on
omega = omega + domega*tfinal; % advance omega to the new time, only changes if J2 on
e_in = e;
M_in = Ma;
Ea=fzero('kepler',Ma); % solve kepler's equation for the EA at the new time
nu = acos((cos(Ea)-e)/(1-e*cos(Ea))); % recalculate the true anomaly
if Ea > pi
nu = 2*pi - nu; % sign check for the arccos
end
[r_ref, v_ref] = orbel2rv(a, e, i, nu, node, omega, MU); % get (r,v) back from the orbital
elements

[t, y] = ode45('conic_de', [0 2*pi*sqrt(a^3/MU)], [r_ref v_ref]);
plot3(y(:,1)/1000, y(:,2)/1000, y(:,3)/1000, 'k', 'linewidth', 2)
xlabel('x (km)')
ylabel('y (km)')
zlabel('z (km)')

figure
hist((stat_data(keep_list,1)-re)/1000,20)
xlabel('Final semi-major axis (km)')
ylabel('Number of particles')
title('Effect of drag on semi-major axis')

figure
hist(stat_data(keep_list,2),20)
xlabel('Final eccentricity')
ylabel('Number of particles')
title('Final eccentricity (due to initial dispersion)')

figure
hist(stat_data(keep_list,3)*180/pi,20)
xlabel('Final inclination (deg)')
ylabel('Number of particles')
title('Final inclination (due to initial dispersion)')

figure
hist(stat_data(keep_list,4)*180/pi,20)
xlabel('Final true anomaly (deg)')
ylabel('Number of particles')
title('Final true anomaly')

figure
hist(stat_data(keep_list,5)*180/pi,20)
xlabel('Final Longitude of ascending node (deg)')
ylabel('Number of particles')
title('Effect of J2 on Longitude of ascending node')

figure
hist(stat_data(keep_list,6)*180/pi,20)
xlabel('Final argument of periapse (deg)')
ylabel('Number of particles')
title('Effect of J2 on argument of periapse')

end

#####
% Calculate the worst case radii of perigee and apogee and out of plane (OOP) for the disk

clear ra rp

ra = stat_data(keep_list,1).*(1 + stat_data(keep_list,2));
rp = stat_data(keep_list,1).*(1 - stat_data(keep_list,2));

ra_max = max(ra);
ra_std = mean(ra) + 3*std(ra); % 3-sigma max radius of apogee
rp_min = min(rp);
rp_std = mean(rp) - 3*std(rp); % 3-sigma max radius of perigee

if i == pi/2
max_oop = max(ra.*sin((stat_data(keep_list,5)-node)));

```

```

    std_oop = 2*(std(ra.*sin( (stat_data(keep_list,5)-node) ));
else
    max_oop = max(ra.*sin( (stat_data(keep_list,3)-i) ));
    std_oop = 2*(std(ra.*sin( (stat_data(keep_list,3)-i) ));
end

if (plot_bounds == 1) & (make_plots == 1) & (disk_volume == 1)
    figure(1)
    hold on
    [a, e, i, nu, node, omega] = rv2orbel(r_ref, v_ref, MU);
    [r_off, v_off]=orbel2rv(rp_min, e, i, nu, node, omega, MU);
    [t, y] = ode45('conic_de',[0 2*pi*sqrt(rp_min^3/MU)], [r_off v_off]);
    offset = max_oop*cross(r_ref, v_ref)/norm(cross(r_ref, v_ref));
    plot3((y(:,1)+offset(1))/1000, (y(:,2)+offset(2))/1000, (y(:,3)+offset(3))/1000,
'r','linewidth', 2)
    plot3((y(:,1)-offset(1))/1000, (y(:,2)-offset(2))/1000, (y(:,3)-offset(3))/1000,
'r','linewidth', 2)

    [r_off, v_off]=orbel2rv(ra_max, e, i, nu, node, omega, MU);
    [t, y] = ode45('conic_de',[0 2*pi*sqrt(ra_max^3/MU)], [r_off v_off]);
    plot3((y(:,1)+offset(1))/1000, (y(:,2)+offset(2))/1000, (y(:,3)+offset(3))/1000,
'r','linewidth', 2)
    plot3((y(:,1)-offset(1))/1000, (y(:,2)-offset(2))/1000, (y(:,3)-offset(3))/1000,
'r','linewidth', 2)

    [r_off, v_off]=orbel2rv(rp_std, e, i, nu, node, omega, MU);
    offset = std_oop*cross(r_ref, v_ref)/norm(cross(r_ref, v_ref));
    [t, y] = ode45('conic_de',[0 2*pi*sqrt(rp_std^3/MU)], [r_off v_off]);
    plot3((y(:,1)+offset(1))/1000, (y(:,2)+offset(2))/1000, (y(:,3)+offset(3))/1000,
'b','linewidth', 2)
    plot3((y(:,1)-offset(1))/1000, (y(:,2)-offset(2))/1000, (y(:,3)-offset(3))/1000,
'b','linewidth', 2)

    [r_off, v_off]=orbel2rv(ra_std, e, i, nu, node, omega, MU);
    [t, y] = ode45('conic_de',[0 2*pi*sqrt(ra_std^3/MU)], [r_off v_off]);
    plot3((y(:,1)+offset(1))/1000, (y(:,2)+offset(2))/1000, (y(:,3)+offset(3))/1000,
'b','linewidth', 2)
    plot3((y(:,1)-offset(1))/1000, (y(:,2)-offset(2))/1000, (y(:,3)-offset(3))/1000,
'b','linewidth', 2)
end

#####
% Calculate the volume and spatial density

if disk_volume == 1
    V_max = 2*max_oop*pi*(ra_max^2 - rp_min^2);
    V_std = 2*std_oop*pi*(ra_std^2 - rp_std^2);
    spatial_d_min = s_objects*(length(keep_list)/objects)/V_max;
    spatial_d_std = s_objects*(length(keep_list)/objects)/V_std;
end

if sshell_volume == 1
    V_max = (4/3)*pi*(ra_max^3 - rp_min^3);
    V_std = (4/3)*pi*(ra_std^3 - rp_std^3);
    spatial_d_min = s_objects*(length(keep_list)/objects)/V_max;
    spatial_d_std = s_objects*(length(keep_list)/objects)/V_std;
end

#####
% Calculate the probability of strike for a particle in the debris field

P_strike_ip_min = 1 - exp(-spatial_d_min*t_mission*Ac*V_rel)
P_strike_ip_std = 1 - exp(-spatial_d_std*t_mission*Ac*V_rel)

if disk_volume == 1
    P_strike_oop_min = (1 - exp(-spatial_d_min*t_mission*Ac*sqrt(2)*V_rel/2)) *
(4*max_oop/(2*pi*a_target))
    P_strike_oop_std = (1 - exp(-spatial_d_std*t_mission*Ac*sqrt(2)*V_rel/2)) *
(4*std_oop/(2*pi*a_target))
end

```

rv2orbel.m

```

function [a, e, i, nu, node, omega]=rv2orbel(r,v,MU)

% function to get these 6 orbital elements from r and v
% (a, e, i, nu, Node, omega)

```

```

h = cross(r,v);          % angular momentum vector
N = cross([0 0 1],h);   % direction of node
evect = (1/MU) * ((norm(v)^2-MU/norm(r))*r - dot(r,v)*v); % eccentricity vector
e = norm(evect);        % magnitude of e
p = (norm(h)^2)/MU;     % the orbit 'parameter'
a = -1/((norm(v)^2)/MU-2/norm(r)); % semimajor axis

i = acos(dot([0 0 1],h)/norm(h)); % inclination

if i==0
    node=0; % node undefined for equatorial, call it zero
else
    node = acos(dot([1 0 0],N)/norm(N)); % calculate node
    if dot(N,[0 1 0]) < 0
        node = 2*pi - node; % quadrant check
    end
end

if ((e==0) | (norm(N)==0))
    omega = 0; % argument of periapse undefined for circular, call it
zero
else
    omega = acos(dot(evect,N)/(e*norm(N))); % calculate argument of periapse
    if dot(evect,[0 0 1]) < 0
        omega = 2*pi - omega; % quadrant check
    end
end

nu = acos(dot(evect,r)/(e*norm(r))); % calculate true anamoly
if dot(r,v) < 0
    nu = 2*pi - nu; % quadrant check
end

```

orbel2rv.m

```

function [r, v] = orbel2rv(a, e, i, nu, node, omega, MU)

% function to get the r and v vectors back from the orbital elements

p = a * (1 - e^2); % orbit parameter
rmag = p/(1 + e*cos(nu)); % magnitude of r at the given 'time'
h = sqrt(p * MU); % magnitude of angular momentum vector
theta = nu + omega; % argument of latitude = true anamoly + argument of periapse

r = rmag*[cos(node)*cos(theta) - sin(node)*sin(theta)*cos(i);
          sin(node)*cos(theta) + cos(node)*sin(theta)*cos(i);
          sin(theta)*sin(i)]; % calculate r

v = -(MU/h)*[cos(node)*(sin(theta)+e*sin(omega)) + sin(node)*(cos(theta) + e*cos(omega))*cos(i);
              sin(node)*(sin(theta)+e*sin(omega)) - cos(node)*(cos(theta) + e*cos(omega))*cos(i);
              -(cos(theta) + e*cos(omega))*sin(i)]; % calculate v

```

kepler.m

```

function out=kepler(E)

global e_in;
global M_in;

out=E-e_in*sin(E)-M_in;

```

conic_de.m

```

function xdot = conic_de(t,x);

global MU_in % m^3/s^2

xdot(1:3,1) = x(4:6,1);
r = x(1:3,1);
rmag = norm(r);
rmag3 = rmag*rmag*rmag;

```

```
xdot(4:6,1)=(-MU_in/rmag3)*r;
```

parse_tle.m

```
clear all

MU = 3.986e14;           % [m^3/s^2], this is for the ****Earth****
re = 6.38e6;            % [m], ****Earth**** radius

fid=fopen('LEO.tle', 'rt')
% fid=fopen('45degmax.tle', 'rt')
count=1;
while 1
    tmp=fgetl(fid);
    if ~ischar(tmp), break, end
    tmp=fgetl(fid);
    if ~ischar(tmp), break, end
    i(count)=str2num(tmp(9:16));
    e(count)=str2num(tmp(27:33))/1e7;
    n(count)=2*pi*str2num(tmp(53:63))/24/3600;    % rad/s
    node(count)=str2num(tmp(18:25));
    count=count+1;
end

fclose(fid);

a=(MU./n.^2).^^(1/3);
alt=(a-re)/1000;        % altitude in [km]

figure
hist(i,20)
xlabel('Inclination (deg)')
ylabel('Number of spacecraft')
title('Inclination survey')

figure
hist(e,20)
xlabel('Eccentricity')
ylabel('Number of spacecraft')
title('Eccentricity survey')

figure
hist(alt,20)
xlabel('Mean Altitude (km)')
ylabel('Number of spacecraft')
title('Altitude survey')

figure
hist(node,20)
xlabel('Ascending Node (deg)')
ylabel('Number of spacecraft')
title('Ascending Node survey')
```

References

-
- ¹<http://www.newsmax.com/archives/articles/2001/2/8/83827.shtml>, *China, Russia Plot Space Attacks*, 2/8/2001
- ² Isakowitz, Steven J., *International Reference Guide to Space Launch Systems*, 3rd Ed., AIAA, 1999, p. 103
- ³ Isakowitz, Steven J., *International Reference Guide to Space Launch Systems*, 3rd Ed., AIAA, 1999, pp. 119-120
- ⁴ Milne, Antony, *Sky Static*, Praeger, 2002, p. 146
- ⁵ Johnson, Nicholas L., *Artificial Space Debris*, Krieger Publishing Co., 1991, pp. 68-69
- ⁶ Milne, Antony, *Sky Static*, Praeger, 2002, p. 138
- ⁷ Weistein, Eric W., <http://mathworld.wolfram.com/SpherePacking.html>, *Sphere Packing*, Wolfram Research, 1999
- ⁸ http://www.iridium.com/corp/iri_corp-story.asp?storyid=2, *About Iridium – Our Story: Corporate Fact Sheet*
- ⁹ http://www.obsat.com/irimage_e.html, Iridium Satellite in Pictures
- ¹⁰ Isakowitz, Steven J., *International Reference Guide to Space Launch Systems*, 3rd Ed., AIAA, 1999, p. 103
- ¹¹ <http://spaceflight.nasa.gov/station/isstodate.html>, *The ISS to date (09/05/03)*, Vital Statistics Section
- ¹² Milne, Antony, *Sky Static*, Praeger, 2002, p. 146
- ¹³ Graves, R., *Space Station Meteoroid and Orbital Debris Survivability*, AIAA-2002-1607, p. 8
- ¹⁴ Graves, R., *Space Station Meteoroid and Orbital Debris Survivability*, AIAA-2002-1607, p. 6, Figure 4
- ¹⁵ Theall, J. R., *Orbital Debris Impacts on Space Shuttle; Model Predictions and Flight Experience*, AIAA 99-0256, p. 2
- ¹⁶ Milne, Antony, *Sky Static*, Praeger, 2002, pp. 148-149
- ¹⁷ Chobotov, Vladimir A. (editor), *Orbital Mechanics*, 2nd Ed., AIAA, 1996, p. 227
- ¹⁸ Wertz, J. R. and Larson, W. J. (editors), *Space Mission Analysis and Design*, 3rd Edition, 1999 Microcosm Press, El Segundo California.
- ¹⁹ Bate, R., Mueller, D., and White, J., *Fundamentals of Astrodynamics*, Dover Publications, Inc., New York, 1971, p. 216
- ²⁰ Battin, Richard. *An Introduction to the Mathematics and Methods of Astrodynamics*, Revised Edition. AIAA, Reston, VA. 1999, p. 125
- ²¹ Chobotov, Vladimir A. (editor), *Orbital Mechanics*, Third Edition, AIAA Educational Series, Reston, VA, 2002, p. 186
- ²² Chobotov, Vladimir A. (editor), *Orbital Mechanics*, Third Edition, AIAA Educational Series, Reston, VA, 2002, p. 228
- ²³ Chobotov, Vladimir A. (editor), *Orbital Mechanics*, Third Edition, AIAA Educational Series, Reston, VA, 2002, p. 315
- ²⁴ Milne, Antony, *Sky Static*, Praeger, 2002, p. 148